Molecules and Cells

Integrated Quantitative Phosphoproteomics and Cell-Based Functional Screening Reveals Specific Pathological Cardiac Hypertrophy-Related Phosphorylation Sites

Hye Kyeong Kwon, Hyunwoo Choi, Sung-Gyoo Park, Woo Jin Park, Do Han Kim, and Zee-Yong Park*

School of Life Sciences, Gwangju Institute of Science and Technology (GIST), Gwangju 61005, Korea
*Correspondence: zeeyong@gist.ac.kr
https://doi.org/10.14348/molcells.2021.4002
www.molcells.org

Cardiac hypertrophic signaling cascades resulting in heart failure diseases are mediated by protein phosphorylation. Recent developments in mass spectrometry-based phosphoproteomics have led to the identification of thousands of differentially phosphorylated proteins and their phosphorylation sites. However, functional studies of these differentially phosphorylated proteins have not been conducted in a large-scale or high-throughput manner due to a lack of methods capable of revealing the functional relevance of each phosphorylation site. In this study, an integrated approach combining quantitative phosphoproteomics and cell-based functional screening using phosphorylation competition peptides was developed. A pathological cardiac hypertrophy model, junctate-1 transgenic mice and control mice, were analyzed using label-free quantitative phosphoproteomics to identify differentially phosphorylated proteins and sites. A cell-based functional assay system measuring hypertrophic cell growth of neonatal rat ventricle cardiomyocytes (NRVMs) following phenylephrine treatment was applied, and changes in phosphorylation of individual differentially phosphorylated sites were induced by incorporation of phosphorylation competition peptides conjugated with cell-penetrating peptides. Cell-based functional screening against 18 selected phosphorylation sites identified three phosphorylation sites (Ser-98, Ser-179 of Ldb3, and Ser-1146 of palladin) displaying near-complete inhibition of cardiac hypertrophic growth of NRVMs. Changes in phosphorylation levels of Ser-98 and Ser-179 in Ldb3 were further confirmed in NRVMs and other pathological/physiological hypertrophy models, including transverse aortic constriction and swimming models, using site-specific phospho-antibodies. Our integrated approach can be used to identify functionally important phosphorylation sites among differentially phosphorylated sites, and unlike conventional approaches, it is easily applicable for large-scale and/or high-throughput analyses.

Keywords: cardiac hypertrophy, cell-based functional screening, neonatal rat ventricle cardiomyocytes, phosphorylation sites, quantitative phosphoproteomics, transgenic mice

INTRODUCTION

Cardiac hypertrophy can be characterized as the response of the heart to various hemodynamic stresses. Chronic mechanical load in the heart resulting from diseases such as arterial hypertension, ischemia, myocardial infarction, vascular dis-

Received 6 January, 2019; accepted 7 January, 2019; published online 23 June, 2021

eISSN: 0219-1032

eases, and familial cardiomyopathy can progress to maladaptive cardiac hypertrophy or heart failure (Tham et al., 2015). Although cardiac hypertrophy is initiated by various receptors at cell membranes sensing biomechanical signals and hormones, it is generally mediated by cellular signaling cascades. Various heart failure disease models have been constructed and investigated, revealing a number of disease-specific cardiac hypertrophic signaling cascades, including beta-adrenergic receptor signaling, Ca^{2+}/calmodulin-dependent kinase II signaling, protein kinase C signaling, mitogen-activated protein kinase signaling, calcineurin-nuclear factor of activated T-cells signaling, cGMP dependent, protein kinase G signaling, and insulin/insulin receptor/AKT (protein kinase B) signaling (Heineke and Molkentin, 2006; Rohini et al., 2010; Shimizu and Minamino, 2016). These hypertrophic cellular signaling pathways ultimately lead to alternations in sarcomere organization, transcription factors, ion channels, and excitation-contraction coupling proteins within cardiomyocytes (Adkins and Curtis, 2015; Kohli et al., 2011; Weeland et al., 2015; Yin et al., 2015).

In general, cellular signaling cascades rely on the sequential activation or inactivation of kinases and phosphatases via protein phosphorylation (Day et al., 2016; Wheeler-Jones, 2005). Protein phosphorylation not only plays a key role in cellular signaling cascades, but also changes the functional state of proteins (Cui et al., 2016; Eom et al., 2011; Lorenz et al., 2009; Ruppert et al., 2013; van Berlo et al., 2011). In cardiac hypertrophy, phosphorylation-dependent functional modulation of proteins, especially sarcoplasmic reticulum (SR) and sarcomere proteins, has been demonstrated. For example, phospholamban, a well-known inhibitor of SERCA2A Ca^{2+} uptake activity, is modulated by specific phosphorylation of Ser-16 and Thr-17 by protein kinase A (PKA) and Ca^{2+}-calmodulin-dependent protein kinase II (CAMKII) (Kranias and Hajjar, 2012; MacLennan and Kranias, 2003; Mattiazzi and Kranias, 2014). Phosphorylation of ryanodine receptor 2 (RyR2) at Ser-2808, Ser-2814, and Ser-2030, mediated by PKA and Ca-CAMKII, is involved in RyR2-mediated SR Ca^{2+} release (Di et al., 2014; Fischer et al., 2015; Li et al., 2013; Respress et al., 2012; Shan et al., 2010a; 2010b). PKA-mediated phosphorylation of cardiac troponin I at Ser-23/24, and cardiac myosin-binding protein-C (cMyBP-C) at Ser-302, also reportedly modulates cardiac contractility (Gresham and Stelzer, 2016; Kooij et al., 2010; Mamidi et al., 2017; Rosas et al., 2015). Additionally, PKA-mediated phosphorylation at Ser-1700 and Thr-1704 of the voltage-gated Ca^{2+} channel Cav 1.2 is involved in excitation-contraction coupling in the heart. Reduced contractility in cardiomyocytes by abnormal phosphorylation results in cardiac hypertrophy over time (Fu et al., 2013; Yang et al., 2016). Notably, all these phosphorylation sites appear to be downstream targets of hypertrophic cellular signaling pathways because kinases activated during hypertrophic cellular signaling, such as PKA and Ca^{2+}-CAMKII, directly phosphorylate these proteins.

To investigate specific cardiac hypertrophic signaling and related cellular processes in various heart failure disease model systems, a large-scale method for quantitative analysis of phosphorylation is required that can provide comprehensive information on differentially phosphorylated proteins and their phosphorylation sites under different conditions. Following recent developments in mass spectrometry (MS)-based quantitative phosphoproteomics, heart disease model-specific cardiac hypertrophic signaling cascades and their related cellular processes have been successfully identified (Chang et al., 2013; Kuzmanov et al., 2016; Lundby et al., 2013; Schechter et al., 2014; Scholten et al., 2013). However, phosphorylation-dependent functionally relevant proteins that could be downstream targets of cardiac hypertrophic signaling cascades are yet to be identified, and the causes of cardiac hypertrophy have not been established. This is primarily due to a lack of high-throughput, large-scale experimental techniques capable of proving the functional relevance of specific phosphorylation sites of cardiac hypertrophy-related proteins by changing individual phosphorylation levels. Construction of genomic mutation models mimicking constitutive activation or null phosphorylation states on single or double phosphorylation sites has been used to study the *in vivo* functional relevance of individual phosphorylation sites (Pollak et al., 2017; Song et al., 2012). However, this approach is not suitable for functional analysis of many phosphorylation sites discovered using quantitative phosphoproteomics approaches.

Herein, we envisaged a cell-based assay system that could alter phosphorylation levels at individual phosphorylation sites of cardiac hypertrophy-related proteins by introducing specific pseudo-substrates of kinases, predicted that it could be used to screen functionally relevant phosphorylation sites, and designed a proof-of-concept experiment. An integrated approach combining quantitative phosphoproteomics discovery and cell-based functional screening to identify functionally important phosphoproteins in cardiac hypertrophy, and their related phosphorylation sites, was subsequently developed. Confirmation of functionally related phosphorylation sites was then carried out by generation of site-specific phospho-antibodies (Fig. 1). In the discovery phase, we performed label-free quantitative phosphorylation analysis of cardiac muscle tissue from a junctate-1-overexpressing transgene (TG) cardiac hypertrophy mouse model to identify cardiac hypertrophy-related phosphoproteins and their phosphorylation sites. Junctate-1 is a high-capacity Ca^{2+}-binding protein localized at the SR membrane (Kwon and Kim, 2009). Several studies have demonstrated that hypertrophied ventricular remodeling is induced by ventricular arrhythmias and atrial fibrillation resulting from alternation of intracellular Ca^{2+} handling capacity (Brandenburg et al., 2016; Lou et al., 2012; Rowin et al., 2017; Seko et al., 2018). Overexpression of junctate-1 in the heart is considered a genetic model of clinically relevant atrial fibrillation, and displays impaired Ca^{2+} transients and arrhythmia, eventually leading to left ventricular hypertrophy as well as cardiac fibrosis (Hong et al., 2008; Nishida et al., 2010). Among differentially phosphorylated phosphopeptides identified using the junctate-1 TG cardiac hypertrophy mouse model, a subset and their phosphorylation sites were selected based on the relevance of cardiac remodeling during cardiac hypertrophy, from evidence including tissue expression patterns (ESTs) and previous functional studies.

In the functional screening phase, we utilized an *in vitro*

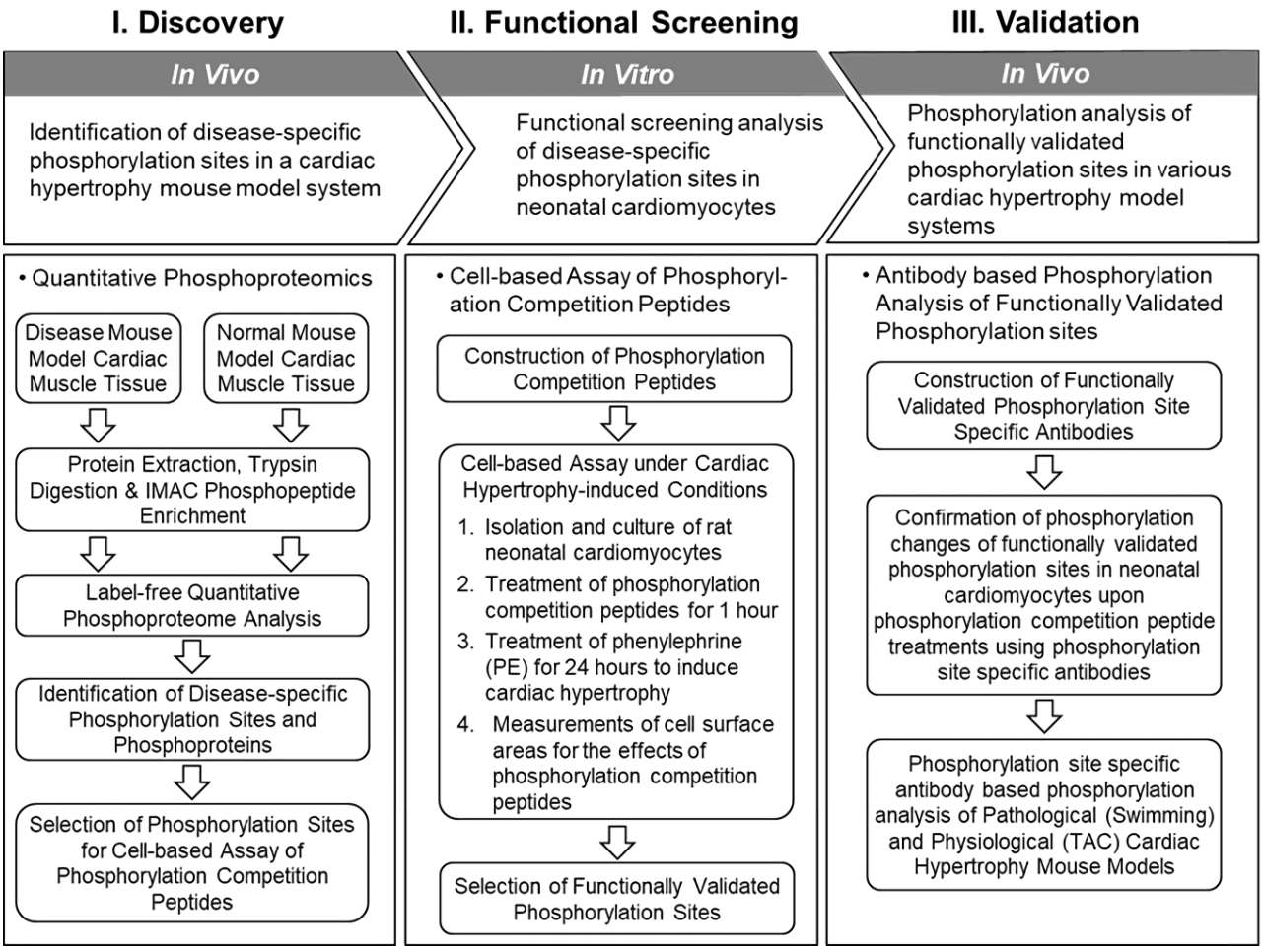

Fig. 1. Overall experimental scheme for screening specific phosphorylation sites involved in cardiac hypertrophy.

cell-based assay system using neonatal rat ventricle cardiomyocytes (NRVMs) that can measure hypertrophic growth upon phenylephrine (PE) treatment. To alter the phosphorylation levels of specific phosphorylation sites of differentially phosphorylated proteins, trans-activator of transcription (TAT) cell-penetrating sequences were conjugated to phosphorylation competition peptides targeting individual phosphorylation sites and incubated with neonatal cardiomyocytes prior to PE treatment. Hypertrophic growth of neonatal cardiomyocytes upon PE treatment was monitored using immunofluorescence to screen functionally relevant phosphorylation sites. Finally, we generated phospho-specific antibodies of functionally relevant phosphorylation sites identified by cell-based functional screening, and changes in phosphorylation levels of individual phosphorylation sites were confirmed in NRVMs and other pathological/physiological hypertrophy models, including transverse aortic constriction (TAC) and swimming models.

MATERIALS AND METHODS

All animal experiments were performed with the approval of the Animal Care Committee of the Gwangju Institute of Science and Technology (No. GIST-2009-14).

Generation of junctate-1 TG mice

To generate junctate-1 overexpression TG mice, mouse junctate-1 cDNA was amplified by PCR using primers 5′-GTT-TTT-TCC-CTT-CTG-TGT-ATT-TTG-TGC-ATG-G (forward) and 5′-CCA-ACT-GAG-CCA-CAG-ATG-CTC-TCA-AAT-AAG-G-3′ (reverse) (Hong et al., 2001). The junctate-1 cDNA was inserted between the 5.4 kb mouse cardiac α-myosin heavy chain promoter and the human growth hormone polyadenylation sequence to generate junctate-1 TG constructs (Palermo et al., 1996). TG mice were produced by Macrogen (Korea) as described previously (Hong et al., 2002). The TG founders were mated with wild-type (WT) FVB/N mice to produce F1 heterozygotes, and F2 homozygotes were produced by cross-mating (Hong et al., 2008). Homozygous 8- to 12-week-old TG and age-matched WT mice were used for this study.

Protein extraction and digestion

Isolated heart left ventricles were washed with ice-cold phosphate-buffered saline (PBS) to remove excess blood, and frozen ventricular tissue was ground with liquid nitrogen using a pre-chilled pestle and mortar. The resultant powder was

collected in Eppendorf tubes and reconstituted in extraction buffer containing 8 M urea, 100 mM TRIS-HCl (pH 8.5), and 1 mM dithiothreitol (DTT). This lysate was sonicated five times at 20% amplitude for 5 s on ice and incubated at 4°C for 1 h. Insoluble debris was removed by centrifugation at 100,000*g* for 1 h, and the protein concentration was determined using a bicinchoninic acid (BCA) assay kit (Thermo Fisher Scientific, USA). After protein mixtures were reduced (5 mM DTT, 30 min) and alkylated with 25 mM iodoacetamide for 30 min in the dark, samples were diluted to 2 M urea with 50 mM TRIS-HCl (pH 8.0) and digested with sequencing grade trypsin (Promega, USA) at a 1:50 enzyme/substrate ratio in the presence of 5 mM $CaCl_2$ at 37°C overnight. Digested peptides were stored at −80°C until use.

Immobilized metal affinity chromatography (IMAC) phosphopeptide enrichment

Phosphopeptide enrichment of mouse heart tissue was carried out as previously described (Choi et al., 2011). Briefly, inline MicroFilters (Upchurch Scientific, USA) were prepared as frits for both a desalting column and a reversed-phase (RP) immobilized metal affinity chromatography (IMAC) phosphopeptide enrichment/trapping column. The desalting column was preparzed using a fused-silica capillary (inner diameter [ID], 250 μm; outer diameter [OD], 360 μm; Polymicro Technologies, USA) packed with 12 cm AQUA C18 resin (5 μm particle size; Phenomenex, USA). The desalting column was sequentially washed with methanol (Fisher Scientific, USA) and solvent B, consisting of 0.1% formic acid (FA; Sigma-Aldrich, USA) and 80% acetonitrile (ACN; Fisher Scientific) in water, and equilibrated with 0.1% FA aqueous solution. Peptide samples were loaded onto the desalting column and washed with at least five column volumes of 1% FA solution. To enrich phosphopeptides, a biphasic trapping column was prepared by packing 3 cm of AQUA C18 resin and 10 cm of IMAC POROS 20 MC resin (Applied Biosystems, USA) into a fused-silica capillary. The column was washed once with solvent B and twice with IMAC binding buffer (40% ACN, 0.1% FA), and connected to the desalting column. After bound peptides were eluted from the desalting column onto the RP/IMAC column with IMAC binding buffer, the desalting column was detached and the RP/IMAC column was washed with IMAC binding buffer to remove non-specifically-bound peptides, and equilibrated with 0.1% trifluoroacetic acid (TFA). Phosphopeptides bound to the IMAC resin were eluted from the 3 cm AQUA C18 RP resin with IMAC elution buffer (100 mM $NH_4H_2PO_4$), and the RP/IMAC column was washed with 0.1% FA. Finally, an analytical column for peptide separation was prepared by pulling a fused-silica capillary (ID, 100 μm; OD, 360 μm; Polymicro Technologies) using a P-2000 laser puller (Sutter Instrument Company, USA) and packing with 7 cm of AQUA C18 resin. The analytical column was connected to the RP/IMAC column for RP liquid chromatography-tandem MS (RPLC-MS/MS) analysis.

LC-MS/MS analysis

Each phosphopeptide sample was analyzed using an Agilent 1100 Series high-performance liquid chromatography (HPLC) pump (Agilent Technologies, USA) coupled to an LTQ linear ion trap mass spectrometer (Thermo Finnigan, USA) using an in house-manufactured nano-electrospray ionization interface with a split flow configuration to adjust the column flow rate to ~250 nl/ml. Solvent A (0.1% FA) and solvent B (0.1% FA, 80% ACN) were used to run a 120 min gradient. The gradient profile started with a 14 min gradient from 0% to 2% solvent B, followed by a 1 min gradient from 2% to 5% solvent B, a 90 min gradient from 5% to 30% solvent B, a 5 min gradient from 30% to 100% solvent B, and a final 10 min gradient of 100% solvent B. Full-scan MS spectra were acquired in the range of 400 to 2,000 *m/z* in data-dependent mode and positive ion mode, with a spray voltage of 2.5 kV. The 10 most abundant ions from each MS scan were selected for further MS/MS analysis using a normalized collision energy of 35%. A dynamic exclusion of 30 s was applied to avoid repeated analysis of the same abundant precursor ion.

Database searching and identification of phosphopeptides

Raw files were searched against UniProt mouse sequence (released on Oct 2, 2015) and decoy databases using the SEQUEST algorithm in Proteome Discoverer Software (ver. 2.2; Thermo Fisher Scientific). SEQUEST parameters were set as fully tryptic peptides with a maximum of two missed cleavages using carbamidomethyl cysteine as a fixed modification (+57 Da), and oxidation of methionine (+16 Da) and phosphorylation of serine, threonine, and tyrosine (+80 Da) as variable modifications. The maximum number of equal modifications allowed per peptide was three. For protein identification, a precursor mass tolerance of 3.0 Da was applied, and the fragment mass tolerance was set as 1.0 Da. A peptide spectral match (PSM) false discovery rate (FDR) of <1% was determined using the target-decoy strategy coupled to Percolator (q-value < 0.01) (Käll et al., 2007). Confident phosphorylation sites were determined using a phosphoRS site localization probability value of >75% (Taus et al., 2011).

Label-free phosphopeptide quantification and bioinformatics

Spectral counts (SpCs) were used for quantification of unique phosphopeptides, which were exported from identified phosphoproteins in Proteome Discoverer according to amino acid sequences and phosphorylated sites for phosphopeptides. To avoid discontinuity in SpC ratios when phosphopeptides had a count of zero, a pseudo-SpC of 0.1 was added to each of these values (Byrum et al., 2013; Patel et al., 2009; Zhang et al., 2013). The 0.1-shifted SpCs were normalized using total SpC (TSpC) to reduce variation between runs as previously described (Gokce et al., 2011). Briefly, for TSpC normalization, the highest number of TSpCs per condition was chosen, and the highest TSpC was divided by the TSpC of each replicate to generate normalization factors (NFs). NFs were then multiplied by each raw SpC value to produce normalized spectral counts (NSpC), and differentially phosphorylated peptides (DPPs) were determined as peptides with a *P* value < 0.05 according to two-tailed Student's *t*-tests, with an absolute $\log_2$ fold change ≥ 0.58 for average NSpCs between WT and TG samples. For SpC definition, undetected peptides had a SpC count of zero; hence only up- and downregulated

phosphopeptides detected in WT or TG samples in at least two out of three replicates were considered DPPs.

Gene Ontology (GO) and Kyoto Encyclopedia of Genes and Genomes (KEGG) pathway analyses were performed using up- and downregulated DPPs identified from the junctate-1 TG 12 week mouse model using Database for Annotation, Visualization and Integrated Discovery (DAVID) software (Huang et al., 2009). GO and KEGG pathway annotations were enriched in DAVID with P values < 0.01, and, with more than three regulated phosphoproteins in each annotation.

Isolation and culturing of NRVMs

NRVMs were obtained from ventricles of 1-day-old Sprague-Dawley rats (Orient Bio, Korea). Cardiomyocytes were isolated and cultured as described previously (Sadoshima et al., 1992). Briefly, minced heart ventricular tissues were digested with HEPES-buffered saline solution containing 0.1% collagen type II (Thermo Fisher Scientific) and 0.4% pancreatin (Sigma-Aldrich) at 37°C. Cardiomyocytes were further purified by Percoll (Amersham Pharmacia Biotech, USA) gradient centrifugation. Cardiomyocytes were plated on collagen-coated dishes (BD Biosciences, USA) and cultured in low-glucose Dulbecco's modified Eagle's medium (DMEM) supplemented with 10% fetal bovine serum (FBS; Hyclone, USA), 2 mM L-glutamine (Invitrogen, USA), and 100 μM 5-bromodeoxyuridine (Sigma-Aldrich) for 24 h.

Phosphorylation competition peptide delivery into isolated neonatal cardiomyocytes

Phosphorylation competition peptides were designed to contain 10 to 15 amino acid residues, with the differentially phosphorylated site identified from phosphorylation analysis of junctate-1 TG mouse hearts in the center of the peptide. Phosphorylation competition peptides were linked to the cell-penetrating peptide sequence of TAT (^{47}YGRKKRRQRRR^{57}) by introducing a cysteine disulfide bond using additional cysteines at the N-terminus of each peptide (Oh et al., 2013). All phosphorylation competition peptides were prepared by AnyGen (Korea) with 95% purity. Prepared cardiomyocytes were starved in serum-free medium overnight and incubated with phosphorylation competition peptides for 1 h.

Immunostaining and measurement of cardiomyocyte surface area

NRVMs plated on collagen-coated glass coverslips were fixed with 4% paraformaldehyde and 4% sucrose in PBS for 7 min, then washed three times with PBS. To permeabilize the membrane, cells were incubated for 10 min with 0.3% Triton X-100 in PBS, then washed in PBS at least three times. Cells were blocked with 5% bovine serum albumin (BSA) for 1 h at room temperature and incubated in monoclonal anti-α-actinin (A7811, 1:200; Sigma-Aldrich) at 4°C overnight, followed by incubation with Alexa Fluor 488 goat anti-mouse IgG (H + L) (A-11001, 1:200; Invitrogen) for 2 h at room temperature. After three subsequent washes, cells were mounted with PermaFluor Aqueous Mounting Medium (Thermo Fisher Scientific). To measure changes in cell surface area, images of cultured cardiomyocytes were visualized by fluorescence microscopy (IX80; Olympus, Japan) using a 20× (0.45 NA) dry objective lens, and cell area was analyzed using ImageJ software (National Institutes of Health, USA). All experiments were performed with three biological replicates. Cardiomyocyte surface area was determined using 50 randomly selected cells per experiment, and calculated as the average cell surface area from each experiment. Average cell surface area was then normalized using the ratio of cell surface area (treated)/cell surface area (untreated). Statistical significance was determined by two-tailed Student's t-tests to estimate significant differences between groups, $P < 0.05$ indicated statistical significance, and mean ± SEM was calculated from three technical replicates.

Cardiac hypertrophy mouse models

Pathological cardiac hypertrophy

Eight-week-old male C57BL/6J mice (body weight, 25-30 g; Orient Bio) were subjected to pressure overload by TAC (or sham operations for controls) for 2 weeks. Mice were anesthetized with 0.3-0.5 ml of Avertin (2,2,2-tribromomethanol; Sigma-Aldrich) working solution, administered by intraperitoneal injection. Avertin stock solution (1.6 mg/ml), prepared by solubilizing in tert-amyl alcohol (Fisher Scientific), was diluted 40-fold with PBS to yield Avertin working solution. Mice were ventilated with a tidal volume of 0.1 ml at a respiratory rate of 120 breaths per min (Harvard Apparatus, USA). A longitudinal incision of 2 to 3 mm was made in the proximal sternum for visualization of the aortic arch. The transverse aortic arch was ligated between the innominate and left common carotid arteries with an overlaid 27-gauge needle. The needle was then immediately removed, leaving a discrete region of constriction (Kho et al., 2011). The sham group was subjected to a similar procedure without ligation.

Physiological cardiac hypertrophy

Exercise training was performed on 8-week-old male C57BL/6J mice (body weight, 28-33 g; Orient Bio) in swimming pools for 2 or 4 weeks. On the first day, training consisted of two 10 min sessions separated by at least 4 h. The exercise intensity of the following endurance training was increased in 10 min increments daily, reaching 90 min, twice daily, whereas untrained mice remained sedentary (Song et al., 2012).

SDS-PAGE and immunoblot analysis

Samples (5 μg) of mouse left ventricle tissue and neonatal cardiomyocyte lysates were prepared by sonication in ice-cold lysis buffer consisting of 10 mM TRIS-HCl (pH 7.5), 1% Triton X-100, 0.1% sodium dodecyl sulfate (SDS), 0.5% sodium cholate, 100 mM NaCl, 1 mM ethylenediaminetetraacetic acid (EDTA), 1 mM ethylene glycol tetraacetic acid (EGTA), protease cocktail inhibitor (Roche, Switzerland), 50 mM NaF, 5 mM Na_3VO_4, 10 mM beta-glycerophosphate, 10 mM sodium pyrophosphate, and 1 mM phenylmethylsulfonyl chloride (PMSF). Soluble lysates were isolated by centrifugation at 13,000g for 1 h to remove insoluble debris, and protein concentrations were determined using a BCA protein assay kit (Thermo Fisher Scientific). Lysates were separated by SDS-polyacrylamide gel electrophoresis (PAGE) on an 8%

polyacrylamide gel and transferred to a PVDF membrane using a mini Trans-Blot Kit (Bio-Rad, USA). The membrane was blocked with 5% BSA for 1 h at room temperature, and incubated with primary antibodies at 4°C overnight. The antibodies and dilutions used for immunoblotting were as follows: 1:10,000 phospho-Ser-98 and phospho-Ser-179 Ldb3 polyclonal antibodies (AbFrontier, Korea); 1:5,000 Cypher (sc-136380; Santa Cruz Biotechnology, USA); and 1:2,500 GAPDH (sc-32233; Santa Cruz Biotechnology). TRIS-buffered saline containing 0.2% Tween-20 (TBS-T) was used as incubating and washing buffer. The membrane was incubated with a 1:20,000 dilution of horseradish peroxidase (HRP)-conjugated goat anti-mouse IgG (115-035-003; Jackson ImmunoResearch, USA) at room temperature for 1 h, and the secondary antibody was visualized on X-ray film by chemiluminescence. Quantification of phosphoproteins was determined by ImageJ software to reveal differences between treated and control groups. Two-tailed Student's *t*-tests were used to establish statistical significance ($P < 0.05$), and mean ± SEM values were estimated from three technical replicates.

Accession code

The mass spectrometry proteomics data have been deposited to the ProteomeXchange Consortium via the PRIDE partner repository with the dataset identifier PXD011421 (Vizcaíno et al., 2016).

RESULTS

Label-free quantitative phosphoproteome analysis of cardiac muscle proteins of junctate-1 TG and control mice

Label-free quantitative phosphoproteome analysis was conducted to monitor changes in protein phosphorylation events in the junctate-1 TG pathological cardiac hypertrophy mouse model. Left ventricle tissue lysates were prepared from 12-week-old junctate-1 TG mice (n = 5) as the pathological cardiac hypertrophy group, and 12-week-old WT mice (n = 5) as the control group. Proteins in solution were digested overnight with trypsin, and phosphopeptides were enriched using an optimized IMAC protocol and subjected to μHPLC-MS/MS analysis. Each group of samples was analyzed with three technical replicates, generating six raw files. Phosphopeptide identification was conducted using Proteome Discoverer with a PSM false discovery rate (FDR) < 0.01 and a Percolator q-value < 0.01. A total of 1,029 phosphopeptides corresponding to 516 phosphoproteins was identified (Supplementary Table S1). To assess the reproducibility of the three technical replicates, normalized spectral counts (NSpCs) were derived by multiplying each raw spectral count (SpC) and NF. NFs were obtained from the ratio of total SpCs (TSpCs) for each replicate and the highest number of TSpCs among technical replicates. Finally, the reproducibility of three technical replicates represented by NSpCs was assessed using average NSpCs of the same group per condition, and errors associated with each technical replicate were estimated using R-squared correction coefficients (R^2). The results are represented in correlation plots for individual NSpCs of WT (R^2 = 0.9366, 0.937, and 0.9256) and TG (R^2 = 0.8059, 0.8726, and 0.9131) groups versus average NSpCs for each group (Supplementary Fig. S1). Next, identified phosphopeptides were re-filtered using a site localization probability >75% (phosphoRS) for each site to confidently select localized phosphorylation sites. Phosphorylation site localization filtering yielded 759 unique phosphopeptides, 428 phosphoproteins, and 886 phosphorylation sites (Fig. 2A). The site localization probabilities for confident phosphopeptides were provided in the highest probability values probability value among individual for unique phosphopeptide in each replicate (Supplementary Table S2). Moreover, we estimated the distribution of each phosphorylation site. Serine was found to be the most abundantly phosphorylated residue (1,100 sites, 85%), followed by threonine (159 sites, 12%), and tyrosine (31 sites, 3%; Supplementary Fig. S2A). Among the 1,029 unique phosphopeptides, 797 were singly phosphorylated. 203 and 29 phosphopeptides contained respectively double and triple phosphorylation sites (Supplementary Fig. S2B). Next, DPPs in junctate-1 TG mice were determined from the changes in NSpCs between junctate-1 TG and WT samples with absolute $\log_2$ fold changes ≥ 0.58 and *P* values < 0.05 (two-tailed Student's *t*-tests). Additionally, phosphopeptides detected in at least two of the three technical replicates in only one condition were selected as DPPs. A total of 227 phosphopeptides (182 upregulated and 45 downregulated phosphopeptides) corresponding to 155 phosphoproteins was significantly differentially regulated in the junctate-1 TG mouse model. The distribution of DPPs is represented as a volcano plot (Fig. 2B), and details of phosphopeptide quantification results are provided as an Excel file in Supplementary Table S1.

GO and KEGG pathway analysis of cellular processes specifically altered in junctate-1 TG mice

GO and KEGG pathway enrichment analyses were performed to reveal cellular processes related to the 155 differentially regulated phosphoproteins. Within GO biological processes (GOBPs), cytoskeleton organization, muscle development, and muscle contraction were identified as the major perturbed processes, and most GOBP annotations were associated with the regulation of cardiac muscle contraction and development (Fig. 2C). Enrichment analysis of GO cellular components (GOCC) showed that most of the regulated phosphoproteins were mainly localized to the contractile fiber, implying that this structure is a critical hotspot for phosphorylation. Subcellular localization analysis revealed that the regulated phosphoproteins were localized to cytoskeleton, vesicle and cytosol (Fig. 2D). Regarding GO molecular function (GOMF), genes related to muscle cytoskeletal functions such as cytoskeleton binding, alpha-actinin binding, and motor activity were enriched. Additionally, Ca^{2+} handling mechanisms (ion channel binding, calmodulin binding) and phosphorylation events (protein kinase binding, phosphatase binding, phosphoprotein binding) were identified as DPPs (Supplementary Fig. S3A). Regarding KEGG pathways, genes related to tight junctions, dilated cardiomyopathy, and hypertrophic cardiomyocytes were significantly expressed (Supplementary Fig. S3B).

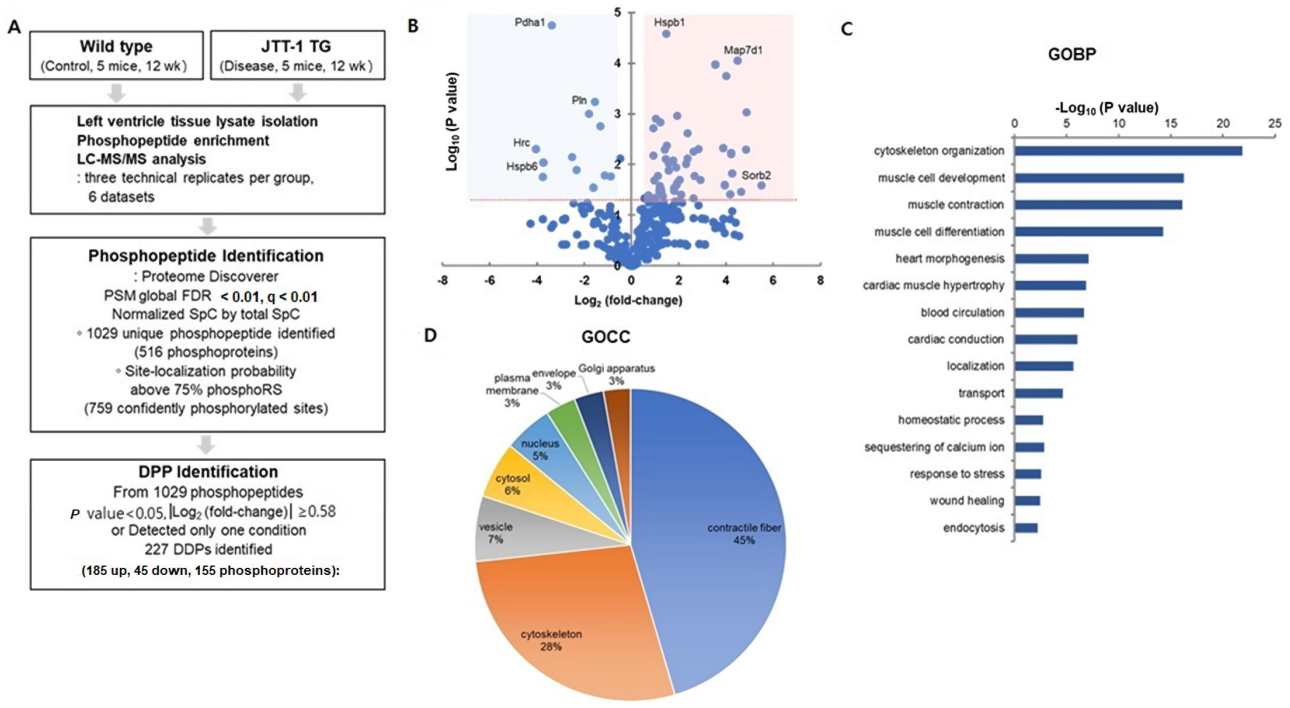

Fig. 2. Identification and functional annotation of DPPs. (A) Left ventricle tissue lysates from 12-week-old JTT-1 transgene (TG) mice (five mice per group, n = 5) were digested, and immobilized Metal Affinity Chromatography (IMAC) phosphopeptide enrichment was performed on the resultant peptides. Enriched phosphopeptides were subjected to μLC-MS/MS. Identified phosphopeptides were normalized using the highest total spectral count (TSpC) for each group and phosphorylation sites with phosphoRS probabilities > 75% were considered to be phosphorylated with a high degree of confidence. Quantification by normalized spectral counts (NSpCs) and selection of DPPs detected uniquely in either of the two groups were used to identify DPPs. Statistically significant differences were determined by performing two-tailed Student's *t*-tests on three technical replicates. (B) The volcano plot of Log_{10} (*P* value) versus Log_2 (fold-change) showed the distribution of DPPs for phosphopeptide quantification using NSpC. Significantly altered DPPs are represented by different colors (red, upregulated; blue, downregulated) and cutoff *P* value ($P < 0.05$) is drawn as a dotted line. (C) Bar chart depicting different Gene Ontology Biological Processes (GOBP) associated with DPPs. (D) Pie chart showing the percentage of Gene Ontology Cellular Component (GOCC) categories of significantly regulated DPPs ($P < 0.01$).

Selection of phosphorylation sites for cell-based functional analysis and construction of phosphorylation competition peptides

Of the differentially phosphorylated sites identified in this study, a subset was selected for subsequent cell-based functional analysis. Out of 155 DPPs, 134 proteins displaying increased phosphorylation levels in pathological cardiac hypertrophy were first considered because lowering the phosphorylation level using phosphorylation completion peptides is expected to be more effective since kinases recognize specific motifs or sequences of substrates. Phosphorylation competition peptides are expected to act as pseudo-substrates of cellular kinases, resulting in decreased phosphorylation of specific phosphorylation sites.

To generate a list of phosphoproteins closely related to cardiac and muscle diseases, the publically available human disease gene network database (https://www.disgenet.org/) was used to identify 47 cardiac- and muscle disease-related genes among the 134 proteins (Fig. 3A). These 47 proteins were further investigated in terms of their tissue-specific ESTs and compared with previously reported cardiac muscle-specific proteome profiles (Lindskog et al., 2015), which reduced the list to 23 proteins. Additional analysis of the literature related to cardiac diseases added a further six proteins to the list. Among the 29 proteins, those not exhibiting changes in protein abundance in the comparative proteome analysis of junctate-1 TG mice and control mice were selected because changes in phosphorylation level of functionally important phosphorylation sites are not accompanied by changes in protein abundance in the same direction (Olsen et al., 2010; Wu et al., 2009; 2011). A total of 14 phosphoprotein was finally selected, and their 18 phosphorylation sites were used for the construction of 16 phosphorylation competition peptides (Supplementary Table S3). To aid incorporation of phosphorylation competition peptides into cells, they were conjugated to the cell-penetrating peptide of the human immunodeficiency virus (HIV) TAT. Phosphorylation competition peptides were 10 to 15 amino acid residues in length, with differentially phosphorylated sites in the center of the peptide, and the cell-penetrating peptide of HIV TAT protein (^{47}YGRKKRRQRRR^{57}) was conjugated via a disulfide bond by adding cysteines at the N-terminus of each peptide.

Cell-based functional screening of specific phosphorylation sites in cardiac hypertrophy-related phosphoproteins

To modulate intracellular phosphorylation levels of specific phosphorylation sites, 18 chemically synthesized TAT-conjugated competition peptides were separately incubated with NRVMs at a final concentration of 100 nM for 1 h, and NRVMs were subsequently exposed to 100 μM PE for 24 h. Next, we investigated whether treatment with site-specific phosphorylation competition peptides altered hypertrophic cell growth by measuring the cell surface area using α-actinin immunostaining. The average cell surface area was measured by fluorescence microscopy of immunostained NRVMs using three independent biological replicates. Following treatment with most phosphorylation competition peptides, PE treatment induced an enlargement of cardiomyocytes by almost 1.8-fold compared with PE-untreated and TAT-treated/PE-untreated controls (Fig. 3B). Meanwhile, PE-induced enlargement of cardiomyocytes was drastically inhibited by pretreatment of competition peptides (^{94}PPIQSPLPVIP^{104} and ^{174}AQGSVSPKVLP^{184}) targeting Ser-98 and Ser-179 of Ldb3 ($P < 0.001$ compared with TAT-treated/PE-treated controls). Since Ldb3 has other major phosphorylation sites that were not identified as differentially phosphorylated sites in the pathological hypertrophy model (Ser-121, Ser-123, Ser-170, and Ser-171), the effects of inhibiting these four phosphorylation sites using two phosphorylation competition peptides (^{117}LATPSPSPEAR^{127} and ^{165}PVAKASSEGAQ^{175}) were also investigated to confirm specific inhibition associated with Ser-98 and Ser-179. Immunofluorescence images of α-actinin following treatment with competition peptides targeting Ser-98 and Ser-179 of Ldb3 revealed less organized actin filament polarity in cells, even after stimulation with PE for 24 h

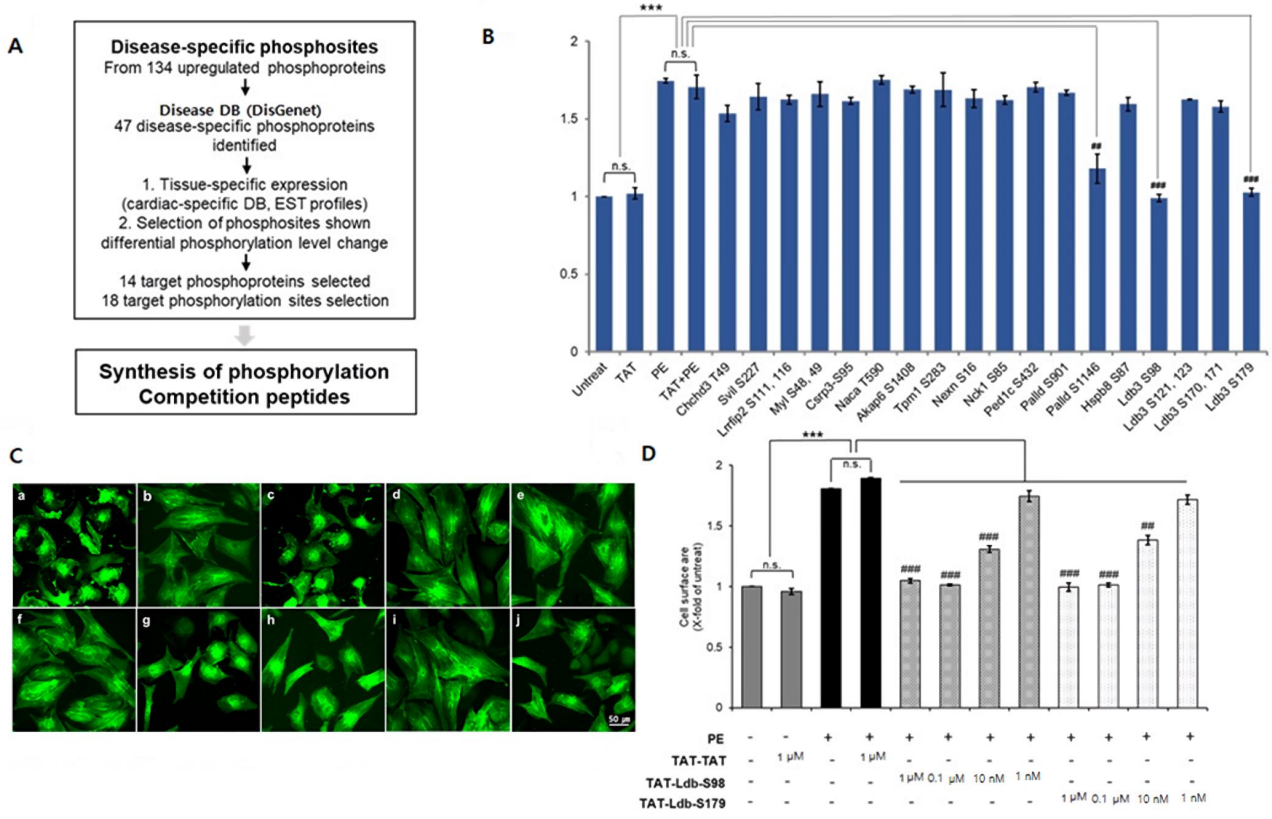

Fig. 3. Site-specific phosphorylation screening by cell-based assay with competition peptides. (A) Overall scheme of disease-specific phosphorylated site selection. Only 47 phosphoproteins among 134 upregulated phosphoproteins were identified as phosphoproteins related to heart and muscle disease in the human disease database. Twenty-nine phosphoproteins were mapped in the heart tissue-specific expression database and literature. The changes at each phosphorylation site were compared with its protein abundance to identify phosphorylation-specific level changes. Finally, 14 target phosphoproteins and phosphorylation competition peptides for 18 phosphorylation target sites were selected for cell-based screening. (B) Cultured neonatal rat cardiomyocytes were treated with 100 nM competition peptides to inhibit site-specific phosphorylation and exposed to 100 μM PE for 24 h. The cell surface area was then determined by immunofluorescence staining of α-actinin, and bar graphs representing surface area were drawn. Statistical significance was assessed by two-tailed Student's *t*-tests for each comparison group with three biological replicates. (C) Immunofluorescence images of sarcomeric α-actinin (a, untreated; b, PE; c, TAT; d, TAT + PE; e, Ldb3-S98 + PE; f, Ldb3-S121, 123 + PE; g, Ldb3-S170, 171 + PE; h, Ldb3-S179 + PE; i, Palld-S901 + PE; j, Pallad-S1146 + PE). PE, phenylephrine; TAT, transactivator of transcription. (D) Bar graphs showing changes in cell surface area following treatment with different concentrations of competition peptides targeting Ser-98 and Ser-179 of Ldb3. ***$P < 0.001$ vs untreated; $^{\#\#}P < 0.01$, $^{\#\#\#}P < 0.001$ vs TAT + PE; n.s., not significant; n = 3 per group.

(Fig. 3C). Additionally, treatment with phosphorylation competition peptides targeting Ser-1146 of palladin inhibited enlargement of the cell surface area by PE ($P < 0.01$) compared with TAT-treated/PE-treated controls. These results indicate that inhibition of phosphorylation on Ser-98 and Ser-179 of Ldb3, and Ser-1146 of palladin, may play a protective role in the PE-induced cardiac hypertrophy model. In addition, we monitored changes in cell surface area following treatment of NRVMs with different concentrations of phosphorylation competition peptides targeting Ldb3 Ser-98 and Ser-179. The inhibitory effects of these two phosphorylation competition peptides were concentration-dependent, yielding complete inhibition of cardiac hypertrophic growth at a concentration of 100 nM (Fig. 3D). These results indicate that our cell-based functional screening system can be used to monitor the functional activities of individual phosphorylation sites. MS/MS spectra matched to corresponding phosphopeptides were manually assigned, and the locations of phosphorylation sites were confirmed by fragment ion analysis (Supplementary Fig. S4).

Generation of site-specific phospho-antibodies for Ser-98 and Ser-179 of Ldb3

In cell-based functional screening of phosphorylation competition peptides, phosphorylation of Ser-98 and Ser-179 in Ldb3 was identified as a strong candidate for modulating cardiac hypertrophic growth ($P < 0.001$). To verify the MS results for these two phosphorylation sites, and monitor changes in phosphorylation level upon treatment with phosphorylation competition peptides, phosphorylation site-specific antibodies were constructed. Rabbit polyclonal phospho-specific antibodies that recognize phosphorylation on Ser-98 and Ser-179 of Ldb3 were generated using synthetic phosphopeptides as antigens. These two phospho-specific antibodies were first tested for their specificity and cross-reactivity. To evaluate reactivity toward Ser-98 and Ser-179 phosphorylation sites in Ldb3, each phospho-antibody was pre-incubated with a mixture of two peptides with the same sequences, whose phosphorylated forms were used as antigens in the generation of phospho-specific antibodies, and junctate-1 TG and control mouse heart lysates used in the discovery phase were probed by immunoblotting. Both phospho-specific antibodies displayed higher reactivity with junctate-1 TG heart lysates, and the reactivity was completely abolished by additional pre-incubation with the respective antigen phosphopeptides. Since both of these phospho-specific antibodies recognize serine phosphorylation, cross-reactivity between the two phosphorylation sites was tested by pre-incubation with opposite antigen phosphopeptides before immunoblotting. Pre-incubation with opposite antigen phosphopeptide did not change the reactivity of either phospho-specific antibody (Supplementary Fig. S5). Next, the reactivity of each phospho-specific antibody toward its specific phosphorylation site was tested by lambda phosphatase treatment of junctate-1 TG and control mouse heart lysates. The reactivity of phospho-specific antibodies was completely lost after lambda phosphatase treatment, indicating that these phospho-specific antibodies recognize only phosphorylated forms of Ldb3 (Supplementary Fig. S6). Taken together, these results demonstrate that two phospho-antibodies are specific for Ldb3 containing phosphorylated Ser-98 and Ser-179, and recognize specific phosphorylation sites of Ldb3.

Phosphorylation of Ser-98 and Ser-179 is altered in junctate-1 TG mice and NRVMs following treatment with phosphorylation competition peptides

Since the site-specific phosphorylation reactivity of phospho-specific antibodies was confirmed, changes in site-specific phosphorylation of Ser-98 and Ser-179 in Ldb3 were monitored using the two phospho-specific antibodies in NRVMs following treatment with phosphorylation competition peptides. An antibody recognizing the intact form of Ldb3 was also used to monitor protein level changes, and the total amount of Ldb3 was not altered under different conditions (Supplementary Fig. S7A). As expected, phosphorylation of Ser-98 was significantly decreased following treatment with a phosphorylation competition peptide targeting Ser-98 under PE-induced hypertrophic conditions, whereas phosphorylation of Ser-98 was not altered upon Ser-179 treatment (Supplementary Fig. S7B). Likewise, phosphorylation of Ser-179 was decreased only upon treatment with the phosphorylation competition peptide targeting Ser-179 under PE-induced hypertrophic conditions (Supplementary Fig. S7C). Furthermore, the decrease in the phosphorylation of these two phosphorylation sites was similar to PE-untreated conditions. These results indicate that the decrease in phosphorylation of Ser-98 and Ser-179 is selectively mediated by treatment with its specific phosphorylation competition peptide, and phosphorylation of these residues may play independent inhibitory roles in cardiac hypertrophy.

Increased phosphorylation of Ser-98 and Ser-179 in Ldb3 was first observed by MS analysis of 12-week-old junctate-1 TG mice. To confirm the MS results, phospho-specific antibodies were used to compare the phosphorylation status of Ser-98 and Ser-179 of Ldb3 at two different time points (8 weeks and 12 weeks) in junctate-1 TG mouse models. A junctate-1 TG mouse model of 8 weeks can be regarded as early stage pathological hypertrophy because expression level changes of E-C coupling proteins such as the L-type Ca^{2+} channel, SERCA2A, PLN, and calsequestrin begin to become visible at this stage (Hong et al., 2008). Thus, it is worth comparing the phosphorylation levels of Ser-98 and Ser-179 in Ldb3 at two different stages of pathological cardiac hypertrophy. An antibody recognizing the intact form of Ldb3 was also included in the immunoblot analysis to monitor changes in protein level, and the intact form of Ldb3 did not exhibit any difference in the amount of protein between junctate-1 TG and control mouse heart lysates at the two time points. A significant increase in phosphorylation of Ser-98 was observed for both 8- and 12-week-old junctate-1 TG mice, and phosphorylation was higher in 12-week-old junctate-1 TG mice. Interestingly, phosphorylation of Ser-179 did not differ much between 8-week-old junctate-1 TG and control mice; a significant increase in phosphorylation of Ser-179 was only observed in 12-week-old junctate-1 TG mice (Fig. 4). Collectively, these results suggest that Ldb3 does not differ at the level of protein abundance, but site-specific phosphorylation changes were evident in pathological hypertrophy models.

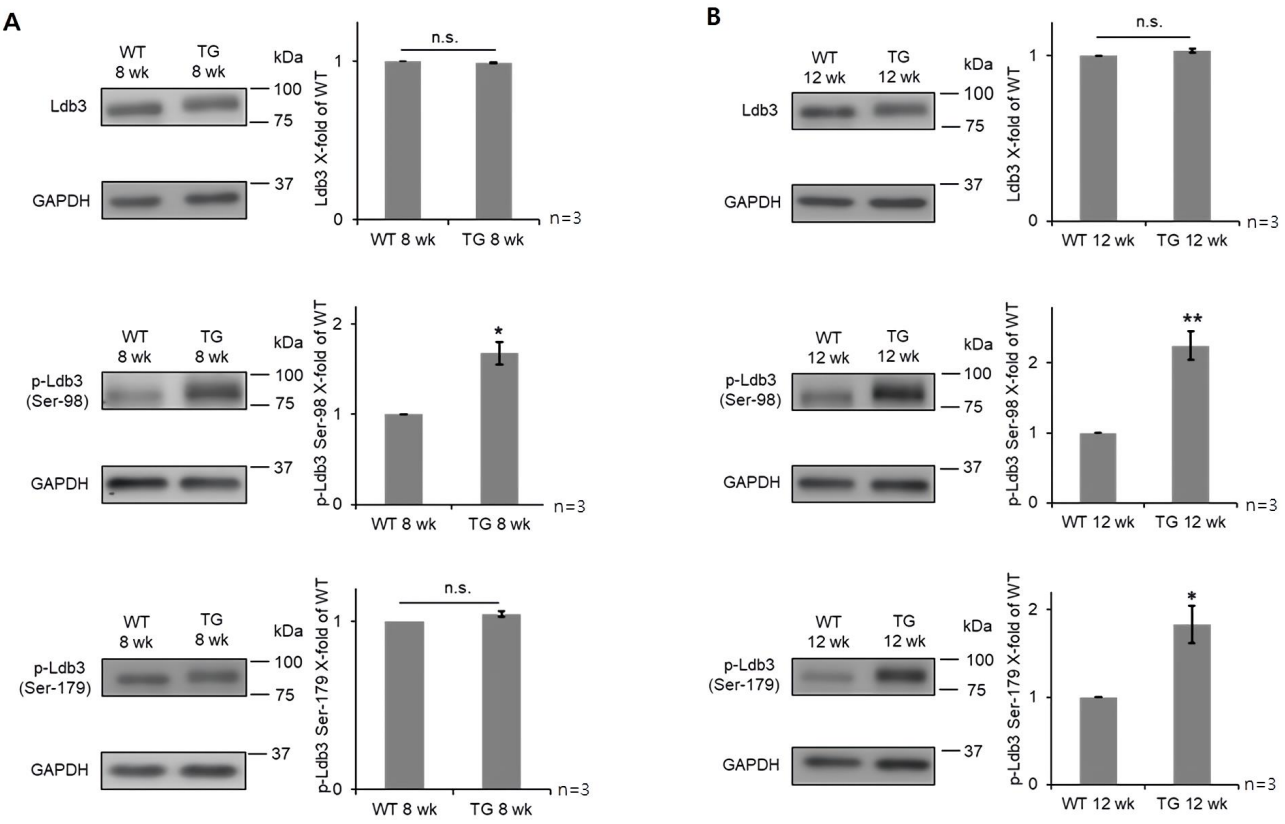

Fig. 4. Changes in site-specific phosphorylation of Ser-98 and Ser-179 of Ldb3 in JTT-1 TG mice. Heart lysates were immunoblotted with non-phospho-antibody, Ser-98 site-specific phospho-antibody, and Ser-179 site-specific phospho-antibody in (A) 8-week-old and (B) 12-week-old JTT-1 TG mice. Bar charts show the relative intensity of site-specific phosphorylation compared with wild-type expression. *P* values determined using two-tailed Student's *t*-tests; $*P < 0.05$, $**P < 0.01$; n.s., not significant; n = 3 per group. Glyceraldehyde-3-phosphate dehydrogenase (GAPDH) served as a loading control.

Phosphorylation of Ldb3 residues Ser-98 and Ser-179 in pathological and physiological cardiac hypertrophy models

Phospho-specific antibodies were used to confirm changes in site-specific phosphorylation of Ldb3 in *in vitro* NRVM primary cells following pathological stimulation (PE) and in an in vivo junctate-1 TG pathological hypertrophy mouse model. To prove whether site-specific changes in phosphorylation of db3 are specific to pathological cardiac hypertrophy, the changes must be further verified in other *in vivo* cardiac hypertrophy models. Two generally accepted models of cardiac hypertrophy were subsequently selected, namely, the swimming-trained mouse physiological hypertrophy model, and the TAC mouse pathological hypertrophy model. We investigated the phosphorylation of Ldb3 in swimming-trained and control mice at two different time points (2 and 4 weeks) to assess physiological cardiac hypertrophy, and at 2 weeks for TAC-operated mice to evaluate pathological cardiac hypertrophy. The levels of Ser-98 and Ser-179 phosphorylation were determined in different cardiac hypertrophy models by immunoblot analysis using phospho-specific antibodies recognizing Ser-98 and Ser-179 in Ldb3. Notably, swimming models did not show any increase in phosphorylation of Ser-98 or Ser-179 up to 4 weeks (Fig. 5A). By contrast, phosphorylation levels of both residues in Ldb3 were significantly increased in the TAC mouse model, and Ser-179 appeared to be phosphorylated to a greater extent than Ser-98 (Fig. 5B). Taken together, these results indicate that increased phosphorylation of Ser-98 and Ser-179 in Ldb3 is specifically associated with pathological cardiac hypertrophy.

DISCUSSION

Combining quantitative phosphoproteomics and cell-based screening with phosphorylation competition peptides identifies functionally relevant phosphorylation sites

In this study, we tested our hypothesis that changes in phosphorylation levels of specific phosphorylation sites could be screened using phosphorylation competition peptides to identify functionally relevant phosphorylation sites in a cell-based assay monitoring hypertrophic growth of NRVMs following PE treatment. Selection of target phosphorylation sites was based on information in cardiac muscle disease gene databases, tissue ESTs, and previous studies reporting relevance to cardiac hypertrophy. Since this study is a proof-of-concept experiment, a modest set of 18 phosphorylation competition peptides covering 22 differentially phosphorylated sites were first tested using the cell-based screening

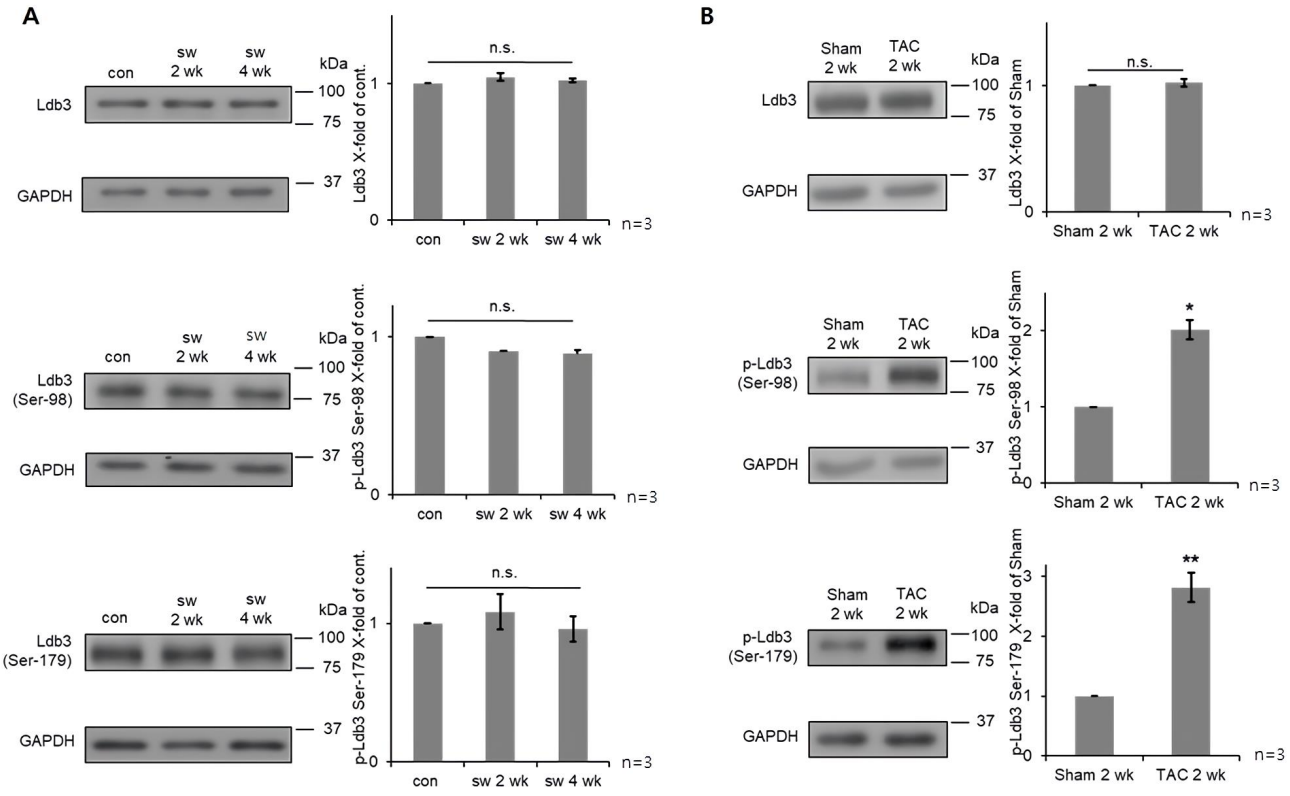

Fig. 5. Phosphorylation of Ser-98 and Ser-179 of Ldb3 is upregulated in pathological specific cardiac hypertrophy. Changes in site-specific phosphorylation of Ser-98 and Ser-179 of Ldb3 were investigated in (A) physiological cardiac hypertrophy (swimming training for 2 or 4 weeks), and (B) pathological cardiac hypertrophy (TAC and sham surgery for 2 weeks). Lysates were probed with non-phospho- and phospho-antibodies (recognizing Ser-98 or Ser-179 of Ldb3) to detect changes in endogenous site-specific phosphorylation. $*P < 0.05$, $**P < 0.01$; n.s., not significant; n = 3 per group. con, control; sw, swimming.

method. Significant inhibition of PE-induced hypertrophic growth of NRVMs was observed using phosphorylation competition peptides targeting Ser-98 and Ser-179 of Ldb3, and Ser-1146 of palladin. Changes in phosphorylation of Ser-98 and Ser-179 of Ldb3 upon treatment with phosphorylation competition peptides were further confirmed using phospho-specific antibodies. Our cell-based functional screening consists of two parts: a cell-based assay monitoring PE-induced hypertrophic growth of NRVMs, and functional screening using TAT sequence-conjugated phosphorylation competition peptides. Monitoring the cell surface area of changes in neonatal cardiomyocytes was employed as a primary parameter to discriminate hypertrophic growth from inhibited hypertrophic growth because NRVMs can display an increase in cell volume and surface area of up to 150% within 48 h of PE treatment (Peter et al., 2016). NRVM imaging has been successfully used to quantify hypertrophic growth in a high-throughput screening method to identify chemical compounds or microRNAs that inhibit cardiac hypertrophic growth (Bass et al., 2012; Jentzsch et al., 2012; Reid et al., 2016; Ryall et al., 2014). Meanwhile, functional analysis using TAT sequence-conjugated phosphorylation competition peptides has been used to modulate site-specific phosphorylation of functionally important proteins without inhibiting cellular kinases or phosphatases following treatment with kinase or phosphatase inhibitors (Du et al., 2012; Oh et al., 2013; Wang et al., 2014). The more conventional approach of phosphomimetic mutation (constitutive activation or null phosphorylation) has also been widely used to modulate site-specific phosphorylation (Ruppert et al., 2013; van Berlo et al., 2011; Yuan et al., 2015). However, whether phosphomimetic mutant proteins carry out their normal functions, and whether expression levels of mutated genes are comparable to those of endogenous proteins, must be confirmed experimentally (Guerra-Castellano et al., 2016; Pondugula et al., 2009). This appears to explain why phosphomimetic mutation analyses targeting well-known phosphorylation sites of cardiac contractility-related proteins such as Ryr2 generate somewhat controversial results (Dobrev and Wehrens, 2014). Furthermore, this approach is not suitable for high-throughput or large-scale screening purposes. Unlike the phosphomimetic mutation approach, TAT sequence-conjugated phosphorylation competition peptides can induce site-specific changes in phosphorylation levels without affecting the cellular activities of kinases and phosphatases, and changes in gene/protein expression levels or loss of functional activity that diminish the usefulness of the phosphomimetic approach are avoided. Thus, functional screening using phosphorylation competition peptides can minimize doubts about whether changes in the pathological state are

solely regulated by site-specific changes in phosphorylation levels. Additionally, this approach can be incorporated into a high-throughput, large-scale screening system. To our knowledge, the present work is the first to demonstrate cell-based functional screening of functionally relevant phosphorylation sites using phosphorylation competition peptides.

Site-specific phosphorylation of Ldb3 and palladin as putative functional modulators in pathological cardiac hypertrophy

Increased phosphorylation of Ser-98 and Ser-179 in Ldb3 was shown to be involved in pathological cardiac hypertrophy *in vitro* using NRVM primary cells, and confirmed *in vivo* using pathological cardiac hypertrophy mouse models. Although previous studies reported the relevance of Ldb3 in pathological cardiac hypertrophy, the present work is the first to associate site-specific phosphorylation of Ldb3 with pathological cardiac hypertrophy. Ldb3, also known as Z-band alternatively spliced PDZ motif (ZASP), Oracle, and Cypher (murine homologue), is a cytoskeletal protein highly expressed in the heart and skeletal muscle in both human and mouse (Faulkner et al., 1999; Huang et al., 2003; Passier et al., 2000). Ldb3 is specifically localized in the Z-line where it is associated with maintaining Z-band integrity during muscle contraction in various species, and Ldb3-null mutant mice suffer neonatal lethality (Benna et al., 2009; van der Meer et al., 2006; Zheng et al., 2009; Zhou et al., 1999; 2001). Ldb3 belongs to the Actin-associated LIM protein (ALP)/Enigma protein family containing an N-terminal PDZ domain as well as one or three LIM domains in its C-terminal region (Zheng et al., 2010). The PDZ domain interacts directly with α-actinin, the major Z-disc cross-linker in sarcomeres, and the PWGFRL motif within the PDZ domain plays a central role in binding to α-actinin (Faulkner et al., 1999; Zhou et al., 1999; 2001). In addition, the PDZ domain of Ldb3 reportedly binds telethonin (T-Cap), forming a protein complex with the sodium channel Na(v)1.5 in human kidney-239 cells and neonatal rat cardiomyocytes (Xi et al., 2012). Several studies also demonstrated that the PDZ region of Ldb3 also interacts with both calsarcin and myotilin in Z-line (Frey and Olson, 2002; Zheng et al., 2009). Notably, the PDZ domain of Zasp52 in Drosophila is crucial in the interaction with α-actinin, and an extended region of ~50 amino acids located at the C-terminus is required for optimum α-actinin binding (Liao et al., 2016). This requirement of the C-terminal extension of the PDZ domain for α-actinin binding was also demonstrated in Alp family proteins (CLP36 and ALP) (Klaavuniemi et al., 2004). Other protein-protein interaction studies reported that the C-terminal extension is involved in determining binding specificity by stabilizing PDZ domain folding (Elkins et al., 2007; Luck et al., 2012; Wang et al., 2010). Interestingly, several studies reported that phosphorylation of the C-terminal extension of the PDZ domain is associated with chaperonin activity for target protein binding. Feng et al. (2003) investigated the interactions of glutamate receptor subunits 2 and 3 (GluR2/3) with multi-PDZ domain glutamate receptor-interacting protein (GRIP), and found that the fourth and fifth PDZ domains, which are packed into a single supramodule via interdomain packing, are required for binding GluR2/3. The authors speculated that phosphorylation of serine residues located in the interdomain linker may play a critical role in destabilizing interdomain packing (Feng et al., 2003). Long et al. (2008) reported that interactions between GRIP1 and cellular matrix proteins Fras1 and Frem2 are mediated by the first two PDZ domains of GRIP1, and phosphorylation of Tyr-134, located in the PDZ1 and PDZ2 interface, may play a detrimental role in the folding of PDZ1, resulting in decreased GRIP1/Fras1 interaction. Zhang et al. (2011) demonstrated that phosphorylation of Tyr-397 located in the C-terminal extension of the PDZ3 domain in postsynaptic density-95 (PSD-95) allosterically regulates the PDZ3 ligand binding affinity, and weakens the interaction of PDZ3 and SH3. In the present study, significantly increased phosphorylation of Ser-98, located in the C-terminal extension of the PDZ domain in Ldb3, was observed in both *in vitro* and *in vivo* pathological cardiac hypertrophy models. Considering the importance of phosphorylation events in the interdomain or linker region, we speculated that changes in the phosphorylation of Ser-98 in Ldb3 may induce conformational changes of the PDZ domain that affect the binding affinity of PDZ ligands such as α-actinin.

The ZASP-like motif (ZM) is another internal region of Ldb3, composed of conserved resides 26 and 27 (Lin et al., 2013; te Velthuis et al., 2007). Several studies showed that the ZM motif is required for binding to the rod region of α-actinin, and for localization of ZM motif-containing PDZ-Lim proteins to the Z-line (Klaavuniemi and Ylänne, 2006; Klaavuniemi et al., 2009). Point mutations at or close to the ZM motif of ZASP/Cypher have been identified in various heart and muscle disease patients (Griggs et al., 2007; Selcen and Engel, 2005; Vatta et al., 2003; Xing et al., 2006; Zhou et al., 2001). Klaavuniemi et al. (2009) found that deletion of a short region at or before the ZM motif of ALP, as well as a point mutation at the conserved Tyr-Ser (YS197-198FA) motif, disrupts localization of ALP to actin stress fibers. The authors speculated that this effect may be dependent on phosphorylation of Tyr197-Ser198. Martinelli et al. (2014) reported that two mutants of the ZM-motif region, A165V and A171T, bind weakly to α-actinin-2 compared with the WT protein. Lin et al. (2014) found that myofibrillar myopathy-associated mutants (A165V and A147T) in the ZM motif-containing actin-binding domain leads to disruption of the Z-disc structure and sarcoplasmic accumulation of actin filaments in skeletal muscle. In the present study, increased phosphorylation of Ser-179 located in the ZM motif of Ldb3 was observed in both *in vitro* and *in vivo* pathological specific hypertrophy models. Considering the importance of the ZM motif for α-actinin binding, we speculated that phosphorylation of Ser-179 may weaken interactions between Ldb3 and α-actinin.

Phosphorylation of Ser-1146 in Palladin was also shown to be involved in pathological cardiac hypertrophy in the present study. Palladin is one of the cytoskeletal proteins responsible for organizing the actin cytoskeleton. It is widely expressed in various cells and tissues, and localizes to stress fibers, focal adhesions, growth cones, embryonic Z-lines, and other actin-based subcellular structures (Otey et al., 2005). Previous studies showed that palladin plays a crucial role in smooth muscle differentiation, migration, contraction, and tissue de-

velopment, and it has been associated with the development of cardiovascular diseases and cancers (Goicoechea et al., 2014; Jin, 2011; McLane and Ligon, 2015; Najm and El-Sibai, 2014). Palladin exists in multiple isoforms, and a common characteristic of all isoforms is the presence of three C-terminal immunoglobulin-like (Ig) domains (Parast and Otey, 2000; Rachlin and Otey, 2006; Wang and Moser, 2008). Since this tandem repeated Ig domain was reported to serve as the binding site for F-actin, studies investigating this interaction have been performed to investigate the role of palladin in the actin cytoskeleton. Dixon et al. (2008) found that the Ig3 domain of palladin binds directly to F-actin, and the tandem Ig3-Ig4 region is able to bundle F-actin. Beck et al. (2013) demonstrated interaction of the Ig3 domain in binding F-actin, and cross-linking of F-actin via electrostatic forces enhances the actin-binding affinity and bundling ability of the tandem Ig3-Ig4 region. Vattepu et al. (2015) proposed that the flexibility of the tandem Ig3-Ig4 linker region induces a critical conformational change in the dimerization of palladin that is important for F-actin binding and bundling. Although the functional relevance of phosphorylation in palladin has not been thoroughly investigated, Akt1-mediated phosphorylation of Ser-507 in the linker region between the Ig3 and Ig4 domains of human palladin was shown to inhibit breast cancer cell migration and promote actin bundling activity (Chin and Toker, 2010). Phosphorylation of human palladin occurs at Ser-507 within the AKT phosphorylation consensus motif (RXRXXS/T) that is highly conserved in other palladin isoforms from different species. Ser-507 in human palladin corresponds to Ser-1143 in the mouse isoform, which also has an RXRXXS motif. Interestingly, Ser-1146 was shown to be the palladin phosphorylation site that inhibited cardiomyocyte hypertrophy in response to PE in the present study. The Ser-1146 phosphorylation is different from the Ser-1143 phosphorylation site and is located close to the original AKT phosphorylation site (three residues distant) within a similar motif sequence (RXRXXXS). Moreover, Ser-1146 is highly conserved in palladin among different species, including human. Due to the presence of multiple arginine residues around Ser-1143 in palladin, phosphorylation of Ser-1143 was not identified by our mass spectrometric analysis. We cannot rule out the possibility of differential phosphorylation of Ser-1143, or changes in Ser-1143 phosphorylation following incubation with phosphorylation competition peptides targeting Ser-1146 (^{1141}SRSRDSGDENE^{1151}). It is still unclear how phosphorylation of Ser-1146 in the tandem Ig3-Ig4 linker region contributes to the role of palladin in regulating pathological cardiac hypertrophy. However, cMyBP-Cs contain three Ig-like domains (C0, C1, and C2) (Craig et al., 2014; Flashman et al., 2004; Luther et al., 2011) at the N-terminus, and an M-domain in the linker region between C0 and C1 that includes four highly conserved serine residues (Jia et al., 2010). Previous studies demonstrated that phosphorylation reduces the extensibility of the M-domain, inducing conformational changes of the N-terminal domain that modulate cardiac contractility (Michalek et al., 2013; Previs et al., 2016). Taken together, these results imply that phosphorylation of the tandem Ig3-Ig4 linker region of palladin may have local or global effects on the palladin structure that influence interactions with multiple binding partners in the actin cytoskeleton. Further studies are needed to elucidate how phosphorylation of Ser-1146 in palladin regulates the development or progression of pathological cardiac hypertrophy.

Note: Supplementary information is available on the Molecules and Cells website (www.molcells.org)

AUTHOR CONTRIBUTIONS

S.G.P., W.J.P., D.H.K., and Z.Y.P. contributed to the study concept and design. H.K.K. and H.C. are responsible for the sample selection and acquisition. H.K.K. and H.C. are in charge of data acquisition. H.K.K., H.C., and Z.Y.P. conducted data analysis. H.K.K. and Z.Y.P. drafted the manuscript. H.K.K. and Z.Y.P. revised the manuscript.

CONFLICT OF INTEREST

The authors have no potential conflicts of interest to disclose.

ORCID

Hye Kyeong Kwon https://orcid.org/0000-0001-8133-0383
Hyunwoo Choi https://orcid.org/0000-0002-1130-9121
Sung-Gyoo Park https://orcid.org/0000-0003-3702-5765
Woo Jin Park https://orcid.org/0000-0002-3236-2212
Do Han Kim https://orcid.org/0000-0002-3390-5469
Zee-Yong Park https://orcid.org/0000-0002-8184-5982

REFERENCES

Adkins, G.B. and Curtis, M.J. (2015). Potential role of cardiac chloride channels and transporters as novel therapeutic targets. Pharmacol. Ther. *145*, 67-75.

Bass, G.T., Ryall, K.A., Katikapalli, A., Taylor, B.E., Dang, S.T., Acton, S.T., and Saucerman, J.J. (2012). Automated image analysis identifies signaling pathways regulating distinct signatures of cardiac myocyte hypertrophy. J. Mol. Cell. Cardiol. *52*, 923-930.

Beck, M.R., Dixon, R.D.S., Goicoechea, S.M., Murphy, G.S., Brungardt, J.G., Beam, M.T., Srinath, P., Patel, J., Mohiuddin, J., Otey, C.A., et al. (2013). Structure and function of Palladin's actin binding domain. J. Mol. Biol. *425*, 3325-3337.

Benna, C., Peron, S., Rizzo, G., Faulkner, G., Megighian, A., Perini, G., Tognon, G., Valle, G., Reggiani, C., Costa, R., et al. (2009). Post-transcriptional silencing of the Drosophila homolog of human ZASP: a molecular and functional analysis. Cell Tissue Res. *337*, 463-476.

Brandenburg, S., Arakel, E.C., Schwappach, B., and Lehnart, S.E. (2016). The molecular and functional identities of atrial cardiomyocytes in health and disease. Biochim. Biophys. Acta *1863*(7 Pt B), 1882-1893.

Byrum, S.D., Larson, S.K., Avaritt, N.L., Moreland, L.E., Mackintosh, S.G., Cheung, W.L., and Tackett, A.J. (2013). Quantitative proteomics identifies activation of hallmark pathways of cancer in patient melanoma. J. Proteomics Bioinform. *6*, 43-50.

Chang, Y.W., Chang, Y.T., Wang, Q., Lin, J.J.C., Chen, Y.J., and Chen, C.C. (2013). Quantitative phosphoproteomic study of pressure-overloaded mouse heart reveals dynamin-related protein 1 as a modulator of cardiac hypertrophy. Mol. Cell. Proteomics *12*, 3094-3107.

Chin, Y.R. and Toker, A. (2010). The actin-bundling protein palladin is an Akt1-specific substrate that regulates breast cancer cell migration. Mol. Cell *38*, 333-344.

Choi, H., Lee, S., Jun, C.D., and Park, Z.Y. (2011). Development of an off-line capillary column IMAC phosphopeptide enrichment method for label-free

phosphorylation relative quantification. J. Chromatogr. B Analyt. Technol. Biomed. Life Sci. *879*, 2991-2997.

Craig, R., Lee, K.H., Mun, J.Y., Torre, I., and Luther, P.K. (2014). Structure, sarcomeric organization, and thin filament binding of cardiac myosin-binding protein-C. Pflugers Arch. *466*, 425-431.

Cui, H., Schlesinger, J., Schoenhals, S., Tönjes, M., Dunkel, I., Meierhofer, D., Cano, E., Schulz, K., Berger, M.F., Haack, T., et al. (2016). Phosphorylation of the chromatin remodeling factor DPF3a induces cardiac hypertrophy through releasing HEY repressors from DNA. Nucleic Acids Res. *44*, 2538-2553.

Day, E.K., Sosale, N.G., and Lazzara, M.J. (2016). Cell signaling regulation by protein phosphorylation: a multivariate, heterogeneous, and context-dependent process. Curr. Opin. Biotechnol. *40*, 185-192.

Di Carlo, M.N., Said, M., Ling, H., Valverde, C.A., De Giusti, V.C., Sommese, L., Palomeque, J., Aiello, E.A., Skapura, D.G., Rinaldi, G., et al. (2014). CaMKII-dependent phosphorylation of cardiac ryanodine receptors regulates cell death in cardiac ischemia/reperfusion injury. J. Mol. Cell. Cardiol. *74*, 274-283.

Dixon, R.D.S., Arneman, D.K., Rachlin, A.S., Sundaresan, N.R., Costello, M.J., Campbell, S.L., and Otey, C.A. (2008). Palladin is an actin cross-linking protein that uses immunoglobulin-like domains to bind filamentous actin. J. Biol. Chem. *283*, 6222-6231.

Dobrev, D. and Wehrens, X.H.T. (2014). Role of RyR2 phosphorylation in heart failure and arrhythmias: controversies around ryanodine receptor phosphorylation in cardiac disease. Circ. Res. *114*, 1311-1319.

Du, J., Wong, W.Y., Sun, L., Huang, Y., and Yao, X. (2012). Protein kinase G inhibits flow-induced Ca2+ entry into collecting duct cells. J. Am. Soc. Nephrol. *23*, 1172-1180.

Elkins, J.M., Papagrigoriou, E., Berridge, G., Yang, X., Phillips, C., Gileadi, C., Savitsky, P., and Doyle, D.A. (2007). Structure of PICK1 and other PDZ domains obtained with the help of self-binding C-terminal extensions. Protein Sci. *16*, 683-694.

Eom, G.H., Cho, Y.K., Ko, J.H., Shin, S., Choe, N., Kim, Y., Joung, H., Kim, H.S., Nam, K.I., Kee, H.J., et al. (2011). Casein kinase-2α1 induces hypertrophic response by phosphorylation of histone deacetylase 2 S394 and its activation in the heart. Circulation *123*, 2392-2403.

Faulkner, G., Pallavicini, A., Formentin, E., Comelli, A., Ievolella, C., Trevisan, S., Bortoletto, G., Scannapieco, P., Salamon, M., Mouly, V., et al. (1999). ZASP: a new Z-band alternatively spliced PDZ-motif protein. J. Cell Biol. *146*, 465-475.

Feng, W., Shi, Y., Li, M., and Zhang, M. (2003). Tandem PDZ repeats in glutamate receptor-interacting proteins have a novel mode of PDZ domain-mediated target binding. Nat. Struct. Biol. *10*, 972-978.

Fischer, T.H., Herting, J., Mason, F.E., Hartmann, N., Watanabe, S., Nikolaev, V.O., Sprenger, J.U., Fan, P., Yao, L., Popov, A.F., et al. (2015). Late INa increases diastolic SR-Ca2+-leak in atrial myocardium by activating PKA and CaMKII. Cardiovasc. Res. *107*, 184-196.

Flashman, E., Redwood, C., Moolman-Smook, J., and Watkins, H. (2004). Cardiac myosin binding protein C: its role in physiology and disease. Circ. Res. *94*, 1279-1289.

Frey, N. and Olson, E.N. (2002). Calsarcin-3, a novel skeletal muscle-specific member of the calsarcin family, interacts with multiple Z-disc proteins. J. Biol. Chem. *277*, 13998-14004.

Fu, Y., Westenbroek, R.E., Scheuer, T., and Catterall, W.A. (2013). Phosphorylation sites required for regulation of cardiac calcium channels in the fight-or-flight response. Proc. Natl. Acad. Sci. U. S. A. *110*, 19621-19626.

Goicoechea, S.M., García-Mata, R., Staub, J., Valdivia, A., Sharek, L., Mcculloch, C.G., Hwang, R.F., Urrutia, R., Yeh, J.J., Kim, H.J., et al. (2014). Palladin promotes invasion of pancreatic cancer cells by enhancing invadopodia formation in cancer-associated fibroblasts. Oncogene *33*, 1265-1273.

Gokce, E., Shuford, C.M., Franck, W.L., Dean, R.A., and Muddiman, D.C. (2011). Evaluation of normalization methods on GeLC-MS/MS label-free spectral counting data to correct for variation during proteomic workflows. J. Am. Soc. Mass Spectrom. *22*, 2199-2208.

Gresham, K.S. and Stelzer, J.E. (2016). The contributions of cardiac myosin binding protein C and troponin I phosphorylation to β-adrenergic enhancement of in vivo cardiac function. J. Physiol. *594*, 669-686.

Griggs, R., Vihola, A., Hackman, P., Talvinen, K., Haravuori, H., Faulkner, G., Eymard, B., Richard, I., Selcen, D., Engel, A., et al. (2007). Zaspopathy in a large classic late-onset distal myopathy family. Brain *130*, 1477-1484.

Guerra-Castellano, A., Díaz-Moreno, I., Velázquez-Campoy, A., De La Rosa, M.A., and Díaz-Quintana, A. (2016). Structural and functional characterization of phosphomimetic mutants of cytochrome c at threonine 28 and serine 47. Biochim. Biophys. Acta *1857*, 387-395.

Heineke, J. and Molkentin, J.D. (2006). Regulation of cardiac hypertrophy by intracellular signalling pathways. Nat. Rev. Mol. Cell Biol. *7*, 589-600.

Hong, C.S., Cho, M.C., Kwak, Y.G., Song, C.H., Lee, Y.H., Lim, J.S., Kwon, Y.K., Chae, S.W., and Kim, D.H. (2002). Cardiac remodeling and atrial fibrillation in transgenic mice overexpressing junctin. FASEB J. *16*, 1310-1312.

Hong, C.S., Kwak, Y.G., Ji, J.H., Chae, S.W., and Kim, D.H. (2001). Molecular cloning and characterization of mouse cardiac junctate isoforms. Biochem. Biophys. Res. Commun. *289*, 882-887.

Hong, C.S., Kwon, S.J., Cho, M.C., Kwak, Y.G., Ha, K.C., Hong, B., Li, H., Chae, S.W., Chai, O.H., Song, C.H., et al. (2008). Overexpression of junctate induces cardiac hypertrophy and arrhythmia via altered calcium handling. J. Mol. Cell. Cardiol. *44*, 672-682.

Huang, C., Zhou, Q., Liang, P., Hollander, M.S., Sheikh, F., Li, X., Greaser, M., Shelton, G.D., Evans, S., and Chen, J. (2003). Characterization and in vivo functional analysis of splice variants of cypher. J. Biol. Chem. *278*, 7360-7365.

Huang, D.W., Sherman, B.T., and Lempicki, R.A. (2009). Systematic and integrative analysis of large gene lists using DAVID bioinformatics resources. Nat. Protoc. *4*, 44-57.

Jentzsch, C., Leierseder, S., Loyer, X., Flohrschütz, I., Sassi, Y., Hartmann, D., Thum, T., Laggerbauer, B., and Engelhardt, S. (2012). A phenotypic screen to identify hypertrophy-modulating microRNAs in primary cardiomyocytes. J. Mol. Cell. Cardiol. *52*, 13-20.

Jia, W., Shaffer, J.F., Harris, S.P., and Leary, J.A. (2010). Identification of novel protein kinase A phosphorylation sites in the M-domain of human and murine cardiac myosin binding protein-C using mass spectrometry analysis. J. Proteome Res. *9*, 1843-1853.

Jin, L. (2011). The actin associated protein palladin in smooth muscle and in the development of diseases of the cardiovasculature and in cancer. J. Muscle Res. Cell Motil. *32*, 7-17.

Käll, L., Canterbury, J.D., Weston, J., Noble, W.S., and MacCoss, M.J. (2007). Semi-supervised learning for peptide identification from shotgun proteomics datasets. Nat. Methods *4*, 923-925.

Kho, C., Lee, A., Jeong, D., Oh, J.G., Chaanine, A.H., Kizana, E., Park, W.J., and Hajjar, R.J. (2011). SUMO1-dependent modulation of SERCA2a in heart failure. Nature *477*, 601-605.

Klaavuniemi, T., Alho, N., Hotulainen, P., Kelloniemi, A., Havukainen, H., Permi, P., Mattila, S., and Ylänne, J. (2009). Characterization of the interaction between Actinin-Associated LIM Protein (ALP) and the rod domain of α-actinin. BMC Cell Biol. *10*, 22.

Klaavuniemi, T., Kelloniemi, A., and Ylänne, J. (2004). The ZASP-like motif in actinin-associated LIM protein is required for interaction with the α-actinin rod and for targeting to the muscle Z-line. J. Biol. Chem. *279*, 26402-26410.

Klaavuniemi, T. and Ylänne, J. (2006). Zasp/Cypher internal ZM-motif containing fragments are sufficient to co-localize with α-actinin--analysis of patient mutations. Exp. Cell Res. *312*, 1299-1311.

Kohli, S., Ahuja, S., and Rani, V. (2011). Transcription factors in heart: promising therapeutic targets in cardiac hypertrophy. Curr. Cardiol. Rev. *7*, 262-271.

Kooij, V., Saes, M., Jaquet, K., Zaremba, R., Foster, D.B., Murphy, A.M., dos Remedios, C., van der Velden, J., and Stienen, G.J.M. (2010). Effect of troponin I Ser23/24 phosphorylation on Ca2+-sensitivity in human myocardium depends on the phosphorylation background. J. Mol. Cell. Cardiol. *48*, 954-963.

Kranias, E.G. and Hajjar, R.J. (2012). Modulation of cardiac contractility by the phopholamban/SERCA2a regulatome. Circ. Res. *110*, 1646-1660.

Kuzmanov, U., Guo, H., Buchsbaum, D., Cosme, J., Abbasi, C., Isserlin, R., Sharma, P., Gramolini, A.O., and Emili, A. (2016). Global phosphoproteomic profiling reveals perturbed signaling in a mouse model of dilated cardiomyopathy. Proc. Natl. Acad. Sci. U. S. A. *113*, 12592-12597.

Kwon, S.J. and Kim, D.H. (2009). Characterization of junctate-SERCA2a interaction in murine cardiomyocyte. Biochem. Biophys. Res. Commun. *390*, 1389-1394.

Li, J., Imtiaz, M.S., Beard, N.A., Dulhunty, A.F., Thorne, R., VanHelden, D.F., and Laver, D.R. (2013). ß-Adrenergic stimulation increases RyR2 activity via intracellular Ca2+ and Mg2+ regulation. PLoS One *8*, e58334.

Liao, K.A., González-Morales, N., and Schöck, F. (2016). Zasp52, a core Z-disc protein in Drosophila indirect flight muscles, interacts with α-actinin via an extended PDZ domain. PLoS Genet. *12*, e1006400.

Lin, C., Guo, X., Lange, S., Liu, J., Ouyang, K., Yin, X., Jiang, L., Cai, Y., Mu, Y., Sheikh, F., et al. (2013). Cypher/ZASP is a novel a-kinase anchoring protein. J. Biol. Chem. *288*, 29403-29413.

Lin, X., Ruiz, J., Bajraktari, I., Ohman, R., Banerjee, S., Gribble, K., Kaufman, J.D., Wingfield, P.T., Griggs, R.C., Fischbeck, K.H., et al. (2014). Z-disc-associated, alternatively spliced, PDZ motif-containing protein (ZASP) mutations in the actin-binding domain cause disruption of skeletal muscle actin filaments in myofibrillar myopathy. J. Biol. Chem. *289*, 13615-13626.

Lindskog, C., Linné, J., Fagerberg, L., Hallström, B.M., Sundberg, C.J., Lindholm, M., Huss, M., Kampf, C., Choi, H., Liem, D.A., et al. (2015). The human cardiac and skeletal muscle proteomes defined by transcriptomics and antibody-based profiling. BMC Genomics *16*, 475.

Long, J., Wei, Z., Feng, W., Yu, C., Zhao, Y.X., and Zhang, M. (2008). Supramodular nature of GRIP1 revealed by the structure of its PDZ12 tandem in complex with the carboxyl tail of Fras1. J. Mol. Biol. *375*, 1457-1468.

Lorenz, K., Schmitt, J.P., Schmitteckert, E.M., and Lohse, M.J. (2009). A new type of ERK1/2 autophosphorylation causes cardiac hypertrophy. Nat. Med. *15*, 75-83.

Lou, Q., Janardhan, A., and Efimov, I.R. (2012). Remodeling of calcium handling in human heart failure. Adv. Exp. Med. Biol. *740*, 1145-1174.

Luck, K., Charbonnier, S., and Trave, G. (2012). The emerging contribution of sequence context to the specificity of protein interactions mediated by {PDZ} domains. FEBS Lett. *586*, 2648-2661.

Lundby, A., Andersen, M.N., Steffensen, A.B., Horn, H., Kelstrup, C.D., Francavilla, C., Jensen, L.J., Schmitt, N., Thomsen, M.B., and Olsen, J.V. (2013). In vivo phosphoproteomics analysis reveals the cardiac targets of β-adrenergic receptor signaling. Sci. Signal. *6*, rs11.

Luther, P.K., Winkler, H., Taylor, K., Zoghbi, M.E., Craig, R., Padron, R., Squire, J.M., and Liu, J. (2011). Direct visualization of myosin-binding protein C bridging myosin and actin filaments in intact muscle. Proc. Natl. Acad. Sci. U. S. A. *108*, 11423-11428.

MacLennan, D.H. and Kranias, E.G. (2003). Phospholamban: a crucial regulator of cardiac contractility. Nat. Rev. Mol. Cell Biol. *4*, 566-577.

Mamidi, R., Gresham, K.S., Li, J., and Stelzer, J.E. (2017). Cardiac myosin binding protein-C Ser 302 phosphorylation regulates cardiac β-adrenergic reserve. Sci. Adv. *3*, e1602445.

Martinelli, V.C., Kyle, W.B., Kojic, S., Vitulo, N., Li, Z., Belgrano, A., Maiuri, P., Banks, L., Vatta, M., Valle, G., et al. (2014). ZASP interacts with the mechanosensing protein Ankrd2 and p53 in the signalling network of striated muscle. PLoS One *9*, e92259.

Mattiazzi, A. and Kranias, E.G. (2014). The role of CaMKII regulation of phospholamban activity in heart disease. Front. Pharmacol. *5*, 5.

McLane, J.S. and Ligon, L.A. (2015). Palladin mediates stiffness-induced fibroblast activation in the tumor microenvironment. Biophys. J. *109*, 249-264.

Michalek, A.J., Howarth, J.W., Gulick, J., Previs, M.J., Robbins, J., Rosevear, P.R., and Warshaw, D.M. (2013). Phosphorylation modulates the mechanical stability of the cardiac myosin-binding protein C motif. Biophys. J. *104*, 442-452.

Najm, P. and El-Sibai, M. (2014). Palladin regulation of the actin structures needed for cancer invasion. Cell Adh. Migr. *8*, 29-35.

Nishida, K., Michael, G., Dobrev, D., and Nattel, S. (2010). Animal models for atrial fibrillation: clinical insights and scientific opportunities. Europace *12*, 160-172.

Oh, J.G., Kim, J., Jang, S.P., Nguen, M., Yang, D.K., Jeong, D., Park, Z.Y., Park, S.G., Hajjar, R.J., and Park, W.J. (2013). Decoy peptides targeted to protein phosphatase 1 inhibit dephosphorylation of phospholamban in cardiomyocytes. J. Mol. Cell. Cardiol. *56*, 63-71.

Olsen, J.V., Vermeulen, M., Santamaria, A., Kumar, C., Miller, M.L., Jensen, L.J., Gnad, F., Cox, J., Jensen, T.S., Nigg, E.A., et al. (2010). Quantitative phosphoproteomics reveals widespread full phosphorylation site occupancy during mitosis. Sci. Signal. *3*, ra3.

Otey, C.A., Rachlin, A., Moza, M., Arneman, D., and Carpen, O. (2005). The palladin/myotilin/myopalladin family of actin-associated scaffolds. Int. Rev. Cytol. *246*, 31-58.

Palermo, J., Gulick, J., Colbert, M., Fewell, J., and Robbins, J. (1996). Transgenic remodeling of the contractile apparatus in the mammalian heart. Circ. Res. *78*, 504-509.

Parast, M.M. and Otey, C.A. (2000). Characterization of palladin, a novel protein localized to stress fibers and cell adhesions. J. Cell Biol. *150*, 643-655.

Passier, R., Richardson, J.A., and Olson, E.N. (2000). Oracle, a novel PDZ-LIM domain protein expressed in heart and skeletal muscle. Mech. Dev. *92*, 277-284.

Patel, P.C., Fisher, K.H., Yang, E.C.C., Deane, C.M., and Harrison, R.E. (2009). Proteomic analysis of microtubule-associated proteins during macrophage activation. Mol. Cell. Proteomics *8*, 2500-2514.

Peter, A.K., Bjerke, M.A., and Leinwand, L.A. (2016). Biology of the cardiac myocyte in heart disease. Mol. Biol. Cell *27*, 2149-2160.

Pollak, A.J., Haghighi, K., Kunduri, S., Arvanitis, D.A., Bidwell, P.A., Liu, G.S., Singh, V.P., Gonzalez, D.J., Sanoudou, D., Wiley, S.E., et al. (2017). Phosphorylation of serine96 of histidine-rich calcium-binding protein by the Fam20C kinase functions to prevent cardiac arrhythmia. Proc. Natl. Acad. Sci. U. S. A. *114*, 9098-9103.

Pondugula, S.R., Brimer-Cline, C., Wu, J., Schuetz, E.G., Tyagi, R.K., and Chen, T. (2009). A phosphomimetic mutation at threonine-57 abolishes transactivation activity and alters nuclear localization pattern of human pregnane X receptor. Drug Metab. Dispos. *37*, 719-730.

Previs, M.J., Mun, J.Y., Michalek, A.J., Previs, S.B., Gulick, J., Robbins, J., Warshaw, D.M., and Craig, R. (2016). Phosphorylation and calcium antagonistically tune myosin-binding protein C's structure and function. Proc. Natl. Acad. Sci. U. S. A. *113*, 3239-3244.

Rachlin, A.S. and Otey, C.A. (2006). Identification of palladin isoforms and characterization of an isoform-specific interaction between Lasp-1 and palladin. J. Cell Sci. *119*, 995-1004.

Reid, B.G., Stratton, M.S., Bowers, S., Cavasin, M.A., Demos-Davies, K.M., Susano, I., and McKinsey, T.A. (2016). Discovery of novel small molecule inhibitors of cardiac hypertrophy using high throughput, high content

imaging. J. Mol. Cell. Cardiol. *97*, 106-113.

Respress, J.L., Van Oort, R.J., Li, N., Rolim, N., Dixit, S.S., Dealmeida, A., Voigt, N., Lawrence, W.S., Skapura, D.G., Skårdal, K., et al. (2012). Role of RyR2 phosphorylation at S2814 during heart failure progression. Circ. Res. *110*, 1474-1483.

Rohini, A., Agrawal, N., Koyani, C.N., and Singh, R. (2010). Molecular targets and regulators of cardiac hypertrophy. Pharmacol. Res. *61*, 269-280.

Rosas, P.C., Liu, Y., Abdalla, M.I., Thomas, C.M., Kidwell, D.T., Dusio, G.F., Mukhopadhyay, D., Kumar, R., Baker, K.M., Mitchell, B.M., et al. (2015). Phosphorylation of cardiac myosin-binding protein-C is a critical mediator of diastolic function. Circ. Heart Fail. *8*, 582-594.

Rowin, E.J., Hausvater, A., Link, M.S., Abt, P., Gionfriddo, W., Wang, W., Rastegar, H., Estes, N.A.M., Maron, M.S., and Maron, B.J. (2017). Clinical profile and consequences of atrial fibrillation in hypertrophic cardiomyopathy. Circulation *136*, 2420-2436.

Ruppert, C., Deiss, K., Herrmann, S., Vidal, M., Oezkur, M., Gorski, A., Weidemann, F., Lohse, M.J., and Lorenz, K. (2013). Interference with ERKThr188 phosphorylation impairs pathological but not physiological cardiac hypertrophy. Proc. Natl. Acad. Sci. U. S. A. *110*, 7440-7445.

Ryall, K.A., Bezzerides, V.J., Rosenzweig, A., and Saucerman, J.J. (2014). Phenotypic screen quantifying differential regulation of cardiac myocyte hypertrophy identifies CITED4 regulation of myocyte elongation. J. Mol. Cell. Cardiol. *72*, 74-84.

Sadoshima, J.I., Jahn, L., Takahashi, T., Kulik, T.J., and Izumo, S. (1992). Molecular characterization of the stretch-induced adaptation of cultured cardiac cells. An in vitro model of load-induced cardiac hypertrophy. J. Biol. Chem. *267*, 10551-10560.

Schechter, M.A., Hsieh, M.K.H., Njoroge, L.W., Thompson, J.W., Soderblom, E.J., Feger, B.J., Troupes, C.D., Hershberger, K.A., Ilkayeva, O.R., Nagel, W.L., et al. (2014). Phosphoproteomic profiling of human myocardial tissues distinguishes ischemic from non-ischemic end stage heart failure. PLoS One *9*, e104157.

Scholten, A., Preisinger, C., Corradini, E., Bourgonje, V.J., Hennrich, M.L., van Veen, T.A.B., Swaminathan, P.D., Joiner, M.L., Vos, M.A., Anderson, M.E., et al. (2013). Phosphoproteomics study based on in vivo inhibition reveals sites of calmodulin-dependent protein kinase II regulation in the heart. J. Am. Heart Assoc. *2*, e000318.

Seko, Y., Kato, T., Haruna, T., Izumi, T., Miyamoto, S., Nakane, E., and Inoko, M. (2018). Association between atrial fibrillation, atrial enlargement, and left ventricular geometric remodeling. Sci. Rep. *8*, 6366.

Selcen, D. and Engel, A.G. (2005). Mutations in ZASP define a novel form of muscular dystrophy in humans. Ann. Neurol. *57*, 269-276.

Shan, J., Betzenhauser, M.J., Kushnir, A., Reiken, S., Meli, A.C., Wronska, A., Dura, M., Chen, B.X., and Marks, A.R. (2010a). Role of chronic ryanodine receptor phosphorylation in heart failure and β-adrenergic receptor blockade in mice. J. Clin. Invest. *120*, 4375-4387.

Shan, J., Kushnir, A., Betzenhauser, M.J., Reiken, S., Li, J., Lehnart, S.E., Lindegger, N., Mongillo, M., Mohler, P.J., and Marks, A.R. (2010b). Phosphorylation of the ryanodine receptor mediates the cardiac fight or flight response in mice. J. Clin. Invest. *120*, 4388-4398.

Shimizu, I. and Minamino, T. (2016). Physiological and pathological cardiac hypertrophy. J. Mol. Cell. Cardiol. *97*, 245-262.

Song, H.K., Hong, S.E., Kim, T., and Kim, D.H. (2012). Deep RNA sequencing reveals novel cardiac transcriptomic signatures for physiological and pathological hypertrophy. PLoS One *7*, e35552.

Song, J., Gao, E., Wang, J., Zhang, X.Q., Chan, T.O., Koch, W.J., Shang, X., Joseph, J.I., Peterson, B.Z., Feldman, A.M., et al. (2012). Constitutive overexpression of phosphomimetic phospholemman S68E mutant results in arrhythmias, early mortality, and heart failure: potential involvement of Na+/Ca2+ exchanger. Am. J. Physiol. Heart Circ. Physiol. *302*, H770-H781.

Taus, T., Köcher, T., Pichler, P., Paschke, C., Schmidt, A., Henrich, C., and Mechtler, K. (2011). Universal and confident phosphorylation site localization using phosphoRS. J. Proteome Res. *10*, 5354-5362.

te Velthuis, A.J.W., Isogai, T., Gerrits, L., and Bagowski, C.P. (2007). Insights into the molecular evolution of the PDZ/LIM family and identification of a novel conserved protein motif. PLoS One *2*, e189.

Tham, Y.K., Bernardo, B.C., Ooi, J.Y.Y., Weeks, K.L., and McMullen, J.R. (2015). Pathophysiology of cardiac hypertrophy and heart failure: signaling pathways and novel therapeutic targets. Arch. Toxicol. *89*, 1401-1438.

van Berlo, J.H., Elrod, J.W., Aronow, B.J., Pu, W.T., and Molkentin, J.D. (2011). Serine 105 phosphorylation of transcription factor GATA4 is necessary for stress-induced cardiac hypertrophy in vivo. Proc. Natl. Acad. Sci. U. S. A. *108*, 12331-12336.

van der Meer, D.L.M., Marques, I.J., Leito, J.T.D., Besser, J., Bakkers, J., Schoonheere, E., and Bagowski, C.P. (2006). Zebrafish cypher is important for somite formation and heart development. Dev. Biol. *299*, 356-372.

Vatta, M., Mohapatra, B., Jimenez, S., Sanchez, X., Faulkner, G., Perles, Z., Sinagra, G., Lin, J.H., Vu, T.M., Zhou, Q., et al. (2003). Mutations in Cypher/ZASP in patients with dilated cardiomyopathy and left ventricular non-compaction. J. Am. Coll. Cardiol. *42*, 2014-2027.

Vattepu, R., Yadav, R., and Beck, M.R. (2015). Actin-induced dimerization of palladin promotes actin-bundling. Protein Sci. *24*, 70-80.

Vizcaíno, J.A., Csordas, A., Del-Toro, N., Dianes, J.A., Griss, J., Lavidas, I., Mayer, G., Perez-Riverol, Y., Reisinger, F., Ternent, T., et al. (2016). 2016 update of the PRIDE database and its related tools. Nucleic Acids Res. *44*, D447-D456.

Wang, C.K., Pan, L., Chen, J., and Zhang, M. (2010). Extensions of PDZ domains as important structural and functional elements. Protein Cell *1*, 737-751.

Wang, H.V. and Moser, M. (2008). Comparative expression analysis of the murine palladin isoforms. Dev. Dyn. *237*, 3342-3351.

Wang, N., Su, P., Zhang, Y., Lu, J., Xing, B., Kang, K., Li, W., and Wang, Y. (2014). Protein kinase D1-dependent phosphorylation of dopamine D1 receptor regulates cocaine-induced behavioral responses. Neuropsychopharmacology *39*, 1290-1301.

Weeland, C.J., van den Hoogenhof, M.M., Beqqali, A., and Creemers, E.E. (2015). Insights into alternative splicing of sarcomeric genes in the heart. J. Mol. Cell. Cardiol. *81*, 107-113.

Wheeler-Jones, C.P.D. (2005). Cell signalling in the cardiovascular system: an overview. Heart *91*, 1366-1374.

Wu, R., Dephoure, N., Haas, W., Huttlin, E.L., Zhai, B., Sowa, M.E., and Gygi, S.P. (2011). Correct interpretation of comprehensive phosphorylation dynamics requires normalization by protein expression changes. Mol. Cell. Proteomics *10*, M111.009654.

Wu, Y.B., Dai, J., Yang, X.L., Li, S.J., Zhao, S.L., Sheng, Q.H., Tang, J.S., Zheng, G.Y., Li, Y.X., Wu, J.R., et al. (2009). Concurrent quantification of proteome and phosphoproteome to reveal system-wide association of protein phosphorylation and gene expression. Mol. Cell. Proteomics *8*, 2809-2826.

Xi, Y., Ai, T., De Lange, E., Li, Z., Wu, G., Brunelli, L., Kyle, W.B., Turker, I., Cheng, J., Ackerman, M.J., et al. (2012). Loss of function of hNav1.5 by a ZASP1 mutation associated with intraventricular conduction disturbances in left ventricular noncompaction. Circ. Arrhythm. Electrophysiol. *5*, 1017-1026.

Xing, Y., Ichida, F., Matsuoka, T., Isobe, T., Ikemoto, Y., Higaki, T., Tsuji, T., Haneda, N., Kuwabara, A., Chen, R., et al. (2006). Genetic analysis in patients with left ventricular noncompaction and evidence for genetic heterogeneity. Mol. Genet. Metab. *88*, 71-77.

Yang, L., Dai, D.F., Yuan, C., Westenbroek, R.E., Yu, H., West, N., de la Iglesia, H.O., and Catterall, W.A. (2016). Loss of β-adrenergic–stimulated

phosphorylation of Ca V 1.2 channels on Ser1700 leads to heart failure. Proc. Natl. Acad. Sci. U. S. A. *113*, E7976-E7985.

Yin, Z., Ren, J., and Guo, W. (2015). Sarcomeric protein isoform transitions in cardiac muscle: a journey to heart failure. Biochim. Biophys. Acta *1852*, 47-52.

Yuan, C.C., Muthu, P., Kazmierczak, K., Liang, J., Huang, W., Irving, T.C., Kanashiro-Takeuchi, R.M., Hare, J.M., and Szczesna-Cordary, D. (2015). Constitutive phosphorylation of cardiac myosin regulatory light chain prevents development of hypertrophic cardiomyopathy in mice. Proc. Natl. Acad. Sci. U. S. A. *112*, E4138-E4146.

Zhang, J., Lanham, K.A., Heideman, W., Peterson, R.E., and Li, L. (2013). Statistically enhanced spectral counting approach to TCDD cardiac toxicity in the adult zebrafish heart. J. Proteome Res. *12*, 3093-3103.

Zhang, J., Petit, C.M., King, D.S., and Lee, A.L. (2011). Phosphorylation of a PDZ domain extension modulates binding affinity and interdomain interactions in postsynaptic density-95 (PSD-95) protein, a membrane-associated guanylate kinase (MAGUK). J. Biol. Chem. *286*, 41776-41785.

Zheng, M., Cheng, H., Banerjee, I., and Chen, J. (2010). ALP / Enigma PDZ-LIM domain proteins in the heart. J. Mol. Cell Biol. *36*, 96-102.

Zheng, M., Cheng, H., Li, X., Zhang, J., Cui, L., Ouyang, K., Han, L., Zhao, T., Gu, Y., Dalton, N.D., et al. (2009). Cardiac-specific ablation of Cypher leads to a severe form of dilated cardiomyopathy with premature death. Hum. Mol. Genet. *18*, 701-713.

Zhou, Q., Chu, P.H., Huang, C., Cheng, C.F., Martone, M.E., Knoll, G., Diane Shelton, G., Evans, S., and Chen, J. (2001). Ablation of Cypher, a PDZ-LIM domain Z-line protein, causes a severe form of congenital myopathy. J. Cell Biol. *155*, 605-612.

Zhou, Q., Ruiz-Lozano, P., Martone, M.E., and Chen, J. (1999). Cypher, a striated muscle-restricted PDZ and LIM domain-containing protein, binds to alpha-actinin-2 and protein kinase C. J. Biol. Chem. *274*, 19807-19813.